

Outward migration of a super-Earth in a disc with outward propagating density waves excited by a giant planet

E. Podlewska-Gaca^{1,3*}, J. C. B. Papaloizou^{2†} and E. Szuszkiewicz^{1,3‡}

¹*Institute of Physics and CASA*, University of Szczecin, ul. Wielkopolska 15, 70-451 Szczecin, Poland*

²*Department of Applied Mathematics and Theoretical Physics, University of Cambridge, Wilberforce Road, Cambridge CB3 0WA, United Kingdom*

³*Kavli Institute for Theoretical Physics, University of California, Santa Barbara, California 93106, USA*

Accepted; Received; in original form

ABSTRACT

In this paper we consider a new mechanism for stopping the inward migration of a low-mass planet embedded in a gaseous protoplanetary disc. It operates when a low-mass planet (for example a super-Earth), encounters outgoing density waves excited by another source in the disc. This source could be a gas giant in an orbit interior to that of the low-mass planet. As the super-Earth passes through the wave field, angular momentum is transferred to the disc material and then communicated to the planet through coorbital dynamics, with the consequence that its inward migration can be halted or even reversed.

We illustrate how the mechanism we consider works in a variety of different physical conditions employing global two-dimensional hydrodynamical calculations. We confirm our results by performing local shearing box simulations in which the super-Earth interacts with density waves excited by an independent harmonically varying potential. Finally, we discuss the constraints arising from the process considered here, on formation scenarios for systems containing a giant planet and lower mass planet in an outer orbit with a 2:1 commensurability such as GJ876.

Key words: planets and satellites: formation - methods: numerical, planet-disc interactions

1 INTRODUCTION

The orbital migration of low-mass planets in protoplanetary discs may play an important role in shaping planetary systems. In our previous studies (Papaloizou & Szuszkiewicz 2005; Podlewska & Szuszkiewicz 2008, 2009; Papaloizou & Szuszkiewicz 2010) we have concentrated on the possibility of the occurrence of a resonant structure during early phases of the evolution of the planetary system. We have considered two-planet systems, containing at least one low-mass planet of several Earth masses, embedded in a gaseous disc. In Podlewska & Szuszkiewicz (2008) we found that in a system with one low-mass planet (described here as a super-Earth) and a gas giant, the formation of commensurabilities readily occurs when the migration of the two planets is convergent with the gas giant being on the larger orbit. However, as shown in Podlewska & Szuszkiewicz (2009), this is no longer true if the migration is convergent but the gas giant is on the smaller orbit. In this case the super-Earth never

gets close enough to the location of the 2:1 commensurability in order to be caught in it. The super-Earth is initially found to migrate towards the central star but at some point stops or even starts to migrate slowly outward. However, no explanation of this phenomenon was given. The aim of our paper is to explore this behavior more fully using both global and local shearing box simulations with the aim of delineating the mechanism responsible for the outward migration, showing how it depends on model parameters such as the mass of the giant planet and the disc aspect ratio.

Since it was realized that the fast migration of low-mass planets (Ward 1997) could pose a serious challenge to scenarios for planet formation, possibilities for slowing down such migration have been the subject of intensive studies. A number of potential mechanisms have been found by focusing on a single low-mass planet embedded in a protoplanetary disc. These mechanisms involve, among others, entry into a magnetospheric cavity close to the star (Lin et al. 1996), effects arising from the orbital eccentricity of a protoplanet (Papaloizou & Larwood 2000), effects due to the possible eccentricity of the protoplanetary disc (Papaloizou 2002), magnetic fields (Terquem 2003), MHD

* E-mail: edytap@univ.szczecin.pl (EP)

† E-mail: J.C.B.Papaloizou@dampt.cam.ac.uk (JP)

‡ E-mail: szusz@fermi.fiz.univ.szczecin.pl (ES)

turbulence (Laughlin, Steinacker & Adams 2004; Nelson & Papaloizou 2004; Johnson, Goodman & Menou 2006; Adams & Bloch 2009), sudden jumps in disc state variables (Menou & Goodman 2004; Matsumura, Pudritz & Thommes 2006), corotation torques (Masset et al. 2006; Paardekooper & Papaloizou 2009a,b), disc thermodynamics (Paardekooper & Mellema 2006; Baruteau & Masset 2008a; Kley & Crida 2008; Paardekooper & Papaloizou 2008; Kley, Bitsch & Klahr 2009; Paardekooper et al. 2010; Hasegawa 2010; Paardekooper et al. 2011; Yamada & Inaba 2011) and instabilities of partial gap edges in low viscosity discs (Li et al. 2009; Yu et al. 2010).

However, there may be mechanisms for affecting migration that depend on having a system of planets. For example, Ogiwara et al. (2010) have suggested the possibility of “an eccentricity trap” operating for a resonantly interacting convoy of planets in a way to halt type I migration near the inner edge of a protoplanetary disc. Thommes (2005) suggested that gas giants may be efficient at capturing low-mass planets in their exterior mean-motion resonances, forming in this way a barrier in a protoplanetary disc “a safety net for fast migrators”. A follow up study based on numerical simulations of the disc planet interactions has been presented by Pierens & Nelson (2008). They found that planets with masses in the range $3.5\text{-}20 M_{\oplus}$ become trapped at the edge of the gap formed by the giant planet, while more massive planets are captured into resonance.

They noted that the positive surface density gradient resembled the configuration discussed by Masset et al. (2006) for their planet trap. Accordingly they raised the possibility that corotation torques operating as in a tidally undisturbed disc could be responsible. However, the configuration differs significantly from that of Masset et al. (2006). The surface density profile in the latter’s planet trap is maintained by a viscosity that increases rapidly inwards. In the absence of a viscous angular momentum flux produced by the action of viscous stresses at an inner boundary, acceleration of the accretion flow would occur, that in turn causes a decrease in the surface density in a steady state. However, in a disc tidally disturbed by a giant planet, the profile is maintained by the outward tidal transport of angular momentum produced by dissipating density waves rather than by either an accretion flow, or effects of comparable magnitude resulting from applied viscous stresses. The wave transport also occurs in the coorbital region of a migrating planet and thus coorbital torques may be expected to behave differently from those occurring in an undisturbed disc. Notably, having an external source of angular momentum for the coorbital region means that positive corotation torques can be sustained without either the action of applied viscous stresses, or the accretion of exterior fresh material into the coorbital zone followed by its loss into the inner regions, which would otherwise be required. Put another way, an external source of angular momentum for the coorbital zone could prevent corotation torques from saturating as would be expected for a tidally undisturbed disc with small applied viscosity. Thus, as seen in our simulations, long term positive torques may be communicated to the planet even when the nominal viscosity is set to zero. In this way, even though there are some similarities, effects seen in a disc that is tidally disturbed by a giant planet may differ from those found in a disc with a

surface density profile maintained through the application of a variable viscosity.

The mechanism, we describe in this paper, operates in a similar physical situation where a low mass planet migrates in a disc which contains trailing density waves excited by another planet. A specific configuration of this type that we consider has a gas giant in an interior orbit with a low mass planet in an exterior orbit around a central mass (see Podlewska & Szuszkiewicz 2009). However, local simulations that we perform indicate that the essential features are a single planet immersed in a field of propagating density waves produced by an external source. The waves are associated with an angular momentum flux which can enter the coorbital region of the low mass planet and transfer angular momentum to the disc material there through the dissipation of shocks. This in turn can transfer angular momentum to the low mass planet through coorbital dynamics. It is important to note that this does not depend on vortensity gradients as do standard corotation torques (e.g. Masset et al. 2006; Paardekooper & Papaloizou 2009a,b). In addition because the waves act as a source of angular momentum from outside the coorbital zone and the transfer involves viscosity independent shock wave dissipation, the usual saturation considerations relevant to standard corotation torques do not apply.

This paper is organized as follows. In Section 2 we describe the physical model and give the basic governing equations. Then in Section 3 we give a brief review of the type I migration theory applicable to an isolated super-Earth embedded in a protoplanetary disc without propagating density waves. We go on to present simulations of a super-Earth embedded in a protoplanetary disc in which density waves excited by an interior giant planet propagate in Section 4. We show that in the presence of outward propagating trailing density waves, the inward type I migration of a super-Earth can be reversed with the consequence that attainment of a 2:1 commensurability by migrating inwards from large radii is prevented. We go on to describe local shearing box simulations of a planet embedded in a disc with density waves excited by an imposed harmonically varying potential in Section 5. We find similar results to those for the global simulations. The waves are found to induce angular momentum transport in the disc material that is then passed on to the planet. In Section 6 we consider this mechanism, which leads to the outward migration of the super-Earth in the global simulations, from the point of view of the conservation of energy and angular momentum. We then consider some consequences of the wave-planet interaction for the resonance capture into an outer 2:1 commensurability of a super-Earth by a gas giant in Section 7. In general density waves excited by the giant planet tend to prevent this, indicating that such commensurabilities, as seen for example in GJ876, may have formed through planetesimal migration after the gas disc dispersed. Finally in Section 8 we give our conclusions.

2 BASIC EQUATIONS AND MODEL

We consider two planets of masses M_1 and M_2 orbiting a central star of mass M_* . We adopt a cylindrical coordinate system (r, ϕ, z) where z is the vertical coordinate increas-

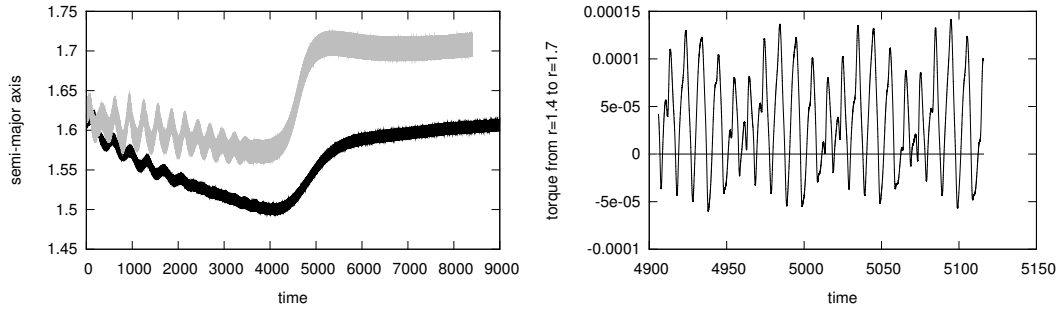


Figure 1. The left panel shows the evolution of the semi-major axis of a super-Earth in a presence of a gas giant with one Jupiter mass (black curve) and two Jupiter masses (grey curve). The right panel shows the variation of the torque acting on the super-Earth: coming from the disc matter located in the vicinity of the planet, in the region between $r = 1.4$ and $r = 1.7$. The timescale covers many periods of the super-Earth, which is located at $r \sim 1.545$ which is close to the azimuthally averaged surface density maximum that occurs slightly exterior to the gap edge. Note during this time period, the giant planet is located at $r \sim 0.9$, to which it has migrated.

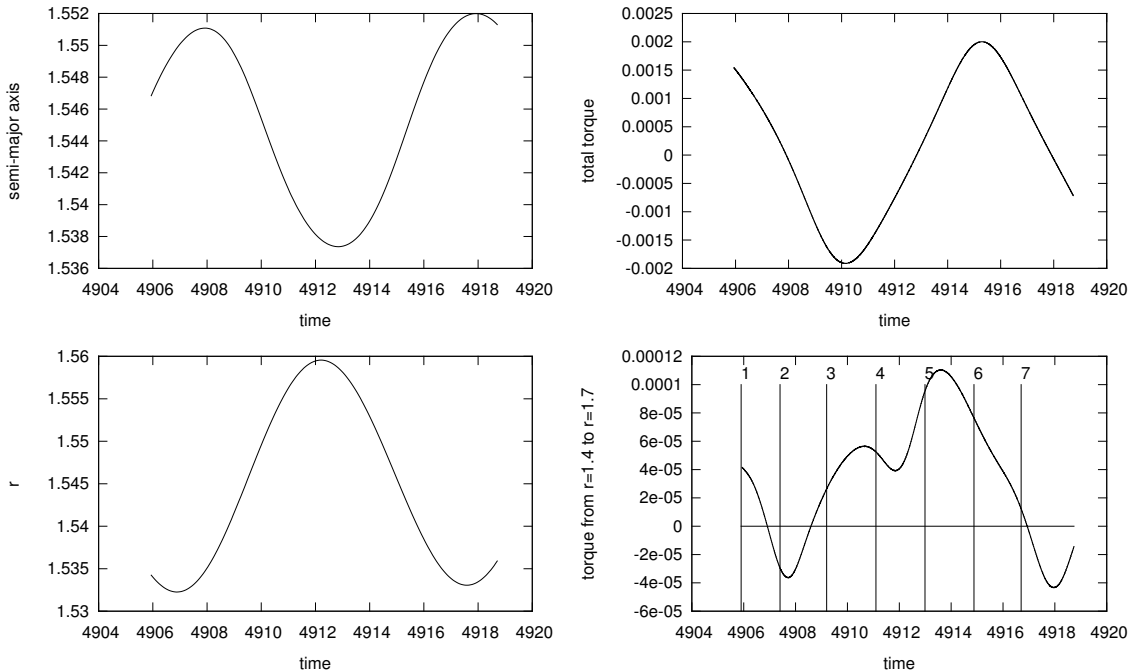


Figure 2. (Left panel) The semi-major axis of the super-Earth (top) and its distance from the central star (bottom) as a function of time. The time interval in each picture corresponds roughly to one orbital period of the super-Earth. (Right panel) The torque acting on the super-Earth: total torque (top), the one coming from the disc matter located in the close vicinity of the planet, namely between $r = 1.4$ and $r = 1.7$ (bottom). The vertical lines in the right bottom panel indicate particular moments of time for which the planet positions in the disc are shown in Fig. 3.

ing in the direction normal to the disc plane for which the unit vector is $\hat{\mathbf{k}}$. We integrate vertically to obtain a two-dimensional flat disc model, for which the governing hydrodynamic equations in an inertial frame are the continuity equation

$$\frac{\partial \Sigma}{\partial t} = -\nabla \cdot (\Sigma \mathbf{u}), \quad (1)$$

and the equation of motion

$$\frac{\partial \mathbf{u}}{\partial t} + \mathbf{u} \cdot \nabla \mathbf{u} = -\frac{1}{\Sigma} \nabla P - \nabla \Phi + \mathbf{f}_\nu, \quad (2)$$

where the vertically integrated pressure is $P = c_s^2(r)\Sigma$ with $c_s(r) = h(GM_*/r)^{1/2}$, and h being the assumed constant

disc aspect ratio. This is related to the putative disc semi-thickness, $H(r)$, through $h = H(r)/r$. Thus a locally isothermal equation of state with sound speed $c_s(r)$ is adopted. The surface density is Σ and \mathbf{u} is the velocity. The viscous force per unit mass is \mathbf{f}_ν . The detailed form of this is given in Nelson et al. (2000). The effective gravitational potential is given by

$$\Phi = -\frac{GM_*}{r} - \sum_{j=1}^2 \left(\frac{GM_j}{\sqrt{r^2 + r_j^2 - 2rr_j \cos(\phi - \phi_j)} + \epsilon_p^2} + \frac{GM_j r}{r_j^2} \cos(\phi - \phi_j) \right). \quad (3)$$

The last term on the right hand side is the indirect term accounting for the acceleration of the primary. In the above, the cylindrical coordinates of the planets that are assumed to be confined to the disc plane are $(r_i, \phi_i, 0)$, $i = 1, 2$ and the softening length is ϵ_p . Note that a non zero value of ϵ_p can be thought of as accounting very approximately for the effects of vertical structure. For the simulations presented here, we adopted $\epsilon_p = 0.024r$. Thus for $h = 0.03$ the softening length is $0.8H$. The corresponding quantities for $h = 0.05$ and $h = 0.07$, for which we have also performed simulations are $0.48H$ and $0.34H$ respectively.

Setting the Keplerian angular velocity to be, $\Omega(r) = (GM_*/r^3)^{1/2}$, the unit of time is taken to be $\Omega(r_{1,0})^{-1}$. Here the gravitational constant is G , M_* denotes the mass of the star and $r_{1,0}$ denotes the initial radial position of the giant planet. The unit of time corresponds to $(1/2\pi)$ times the orbital period of the initial orbit of the inner giant planet. The adopted unit of length is the initial orbital radius of the giant planet which can be assumed to correspond to 5.2 au. However, it may be scaled from this to arbitrary values by applying a scaling factor, λ , provided that the disc surface density is scaled by λ^{-2} preserving the mass scale. The unit of time then scales as $\lambda^{3/2}$.

We consider discs which undergo near-Keplerian rotation with H being small compared to r . We have adopted two initial surface density profiles for the disc. For the standard initial disc, which was adopted below unless stated otherwise, the profile was taken to be uniform with $\Sigma = \Sigma_0$ in the vicinity of the super-Earth with tapers at inner and outer radii prescribed according to

$$\begin{aligned} \Sigma &= (0.1 + 4.5(r - r_{min}))\Sigma_0 & \text{for } r < r_{min} + 0.2, \\ \Sigma &= \Sigma_0 & \text{for } r_{min} + 0.2 \leq r < 1.65, \\ \Sigma &= \Sigma_0 \times (r/1.65)^{-1.5} & \text{for } r > 1.65, \end{aligned} \quad (4)$$

where r_{min} being the inner edge of the disc was taken to be 0.33.

Some of our simulations were carried out for an initial disc with a more extensive uniform surface density region, with as before, exterior and interior tapers but also a region of low surface density in the vicinity of the orbital radius of the giant planet, corresponding to a gap. The surface density was given by

$$\begin{aligned} \Sigma &= (0.1 + 4.5(r - r_{min}))\Sigma_0 & \text{for } r < r_{min} + 0.2, \\ \Sigma &= \Sigma_0 & \text{for } r_{min} + 0.2 \leq r < 0.7, \\ \Sigma &= \Sigma_0 \times (r/0.65)^{-11.25} & \text{for } 0.7 \leq r < 0.75, \\ \Sigma &= 0.001\Sigma_0 & \text{for } 0.75 \leq r < 1.15, \\ \Sigma &= \Sigma_0 \times (r/1.43)^{11.25} & \text{for } 1.15 \leq r < 1.43, \\ \Sigma &= \Sigma_0 & \text{for } 1.43 \leq r < 4.3, \\ \Sigma &= \Sigma_0 \times (r/4.3)^{-1.5} & \text{for } r > 4.3. \end{aligned} \quad (5)$$

This disc is referred to below as the one having a more extensive uniform surface density region. We remark that, due to nonlinear perturbations from the giant planet the surface density profile, in the vicinity of and interior to the low mass planet, tends to relax quickly to a form that does not depend on the initial profile used. However, differences at larger radii may remain throughout the simulations.

In practice we adopted $\Sigma_0 = 6 \times 10^{-4} M_\odot / (5.2au)^2$ which, for $M_* = M_\odot$, corresponds to the minimum mass solar nebula (MMSN) with two Jupiter masses contained within a

circular area of radius equal to $5.2au$. Note that results may be scaled to different values of M_* by multiplying the planet masses by M_*/M_\odot and surface densities and radii by $(M_*/M_\odot)^{1/3}$. The mass M_1 is taken to be that of a giant planet and the mass M_2 is taken to be that of a super-Earth. All planets are initialized on circular orbits.

We used the Eulerian hydrodynamic code NIRVANA (Ziegler 1998) to solve the governing equations as was done in our previous papers (Papaloizou & Szuszkiewicz 2005; Podlewska & Szuszkiewicz 2008, 2009). The details of the numerical scheme can be found in Nelson et al. (2000). The computational domain in the radial direction extends from $r_{min} = 0.33$ to r_{max} , which has been taken to be in the range 4 – 5. The azimuthal angle φ lies in the interval $[0, 2\pi]$. The disc domain is partitioned into grid cells in such a way that a single grid cell is approximately square with sides parallel to the radial and azimuthal directions being approximately equal to 0.01 in dimensionless units. The radial boundaries were taken to be open.

When calculating the gravitational forces on the planets due to the disc, we include the matter contained in the planet's Hill spheres. We remark that in practice only the super-Earth is enveloped by the disc and for such a low-mass planet, the influence of the material inside Hill sphere can in any case be neglected. The self-gravity of the disc is neglected.

We have run our numerical experiments with disc aspect ratio, h , ranging from 0.03 to 0.07 and constant kinematic viscosity ν . Unless stated otherwise, we have adopted $\nu = 2 \times 10^{-6}$ in dimensionless units (this corresponds to the standard α parameter being equal to 2.2×10^{-3} for $h = 0.03$, 8×10^{-4} for $h = 0.05$ and 4.1×10^{-4} for $h = 0.07$).

3 AN ISOLATED SUPER-EARTH EMBEDDED IN A PROTOPLANETARY DISC

The migration of low-mass planets in a gaseous disc has been calculated from the linear response of the disc to the perturbation caused by the presence of a planet (e.g. Tanaka et al. 2002). This procedure is reasonable if coorbital torques do not play a role. The latter depend on the disc surface density and temperature profiles and thermodynamics. When they are important, non-linear effects play a role (Paardekooper et al. 2011; Yamada & Inaba 2011). According to the recent studies, a single low-mass planet can migrate with a whole range of speeds, both inwards and outwards, depending on the assumed physical and structural properties of the disc in which it is embedded.

For the disc models we consider, a super-Earth with the mass of $5.5 M_\oplus$ orbiting the Solar-mass star embedded in such a disc undergoes inward migration with a speed similar to that derived from the linear treatment of Tanaka et al. (2002). The situation is very different if the super-Earth migrates in a disc in which density waves excited by a gas giant are present and have a significant interaction with it. We go on to consider this situation below.

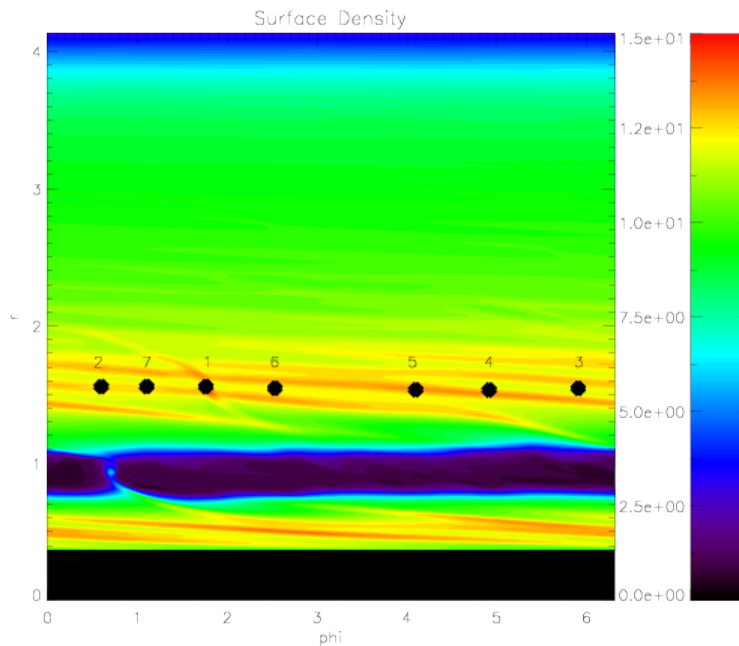


Figure 3. The surface density contours in the disc at a time denoted by 1. The wake associated with the super-Earth can be clearly seen. The planet positions at six additional times denoted 2 – 7 are correspondingly marked to indicate their relation to the wave pattern excited by the Jupiter mass planet. The times correspond to those indicated in Fig. 2 (right bottom panel), for which the values of torques have been given. The Jupiter mass planet is at fixed azimuthal position as would be situation in a frame that corotates with it.

4 A SUPER-EARTH EMBEDDED IN A PROTOPLANETARY DISC IN WHICH DENSITY WAVES EXCITED BY AN INTERIOR GIANT PLANET PROPAGATE

Before considering the migration of the super-Earth, we briefly review some well known relevant properties of the density waves excited in a gaseous disc by an orbiting giant planet.

4.1 Density waves excited by a giant planet

It is well known that an orbiting planet or satellite excites density waves in a nearby gaseous disc that is orbiting the same central body (Goldreich & Tremaine 1979). The density waves are launched at Lindblad resonances and propagate away from the planet where they eventually shock and dissipate. Because of this they take the form of trailing waves propagating away from the planet which are always associated with outward angular momentum transport (e.g. Lynden-Bell & Kalnajs 1972; Balbus & Papaloizou 1999).

For a non migrating or slowly migrating protoplanet embedded in a disc without density waves viewed in a frame rotating with the mean angular velocity of the planet, there are closed streamlines that represent a coorbital flow. Each of these can be thought of as constituting a single coorbital cell that occupies almost the full 2π in azimuth, with the protoplanet located in the excluded region (see for example the ‘librating streamlines’ in Fig. 5 of Masset & Papaloizou (2003)). This of course is the same situation that occurs

in particle dynamics without pressure where the librating orbits correspond to horseshoe orbits.

When density waves are present, the coorbital flows may be significantly affected by general pressure forces and shock waves such they depart from the normal horseshoe form. However, if fluid elements still remain trapped in the coorbital region, dissipative effects acting on the coorbital flow can lead to a net force or torque acting on the super-Earth, a phenomenon that will be discussed further in Sections 4.2 and 6.2 below.

This is analogous to the situation that occurs for particles that are subject to secular dissipative forces that cause them to slowly migrate in the absence of the protoplanet. When a non migrating low mass protoplanet that induces horseshoe trajectories is present, particles on those trajectories can become trapped, communicating the dissipative forces/torques that act on them to the protoplanet (e.g. Dermott et al. 1980).

In order for this phenomenon to result in a positive torque on the protoplanet, the local dissipation of the waves, in practice mostly through shocks, should produce a positive torque on the disc material, as is indeed expected for trailing density waves excited by an interior giant planet. Furthermore this transport should exceed any counteracting effects produced by a disc viscosity on average, in order for a net positive torque to be communicated to the protoplanet. Thus the torques associated with the dissipation of the density waves should exceed viscous torques, implying

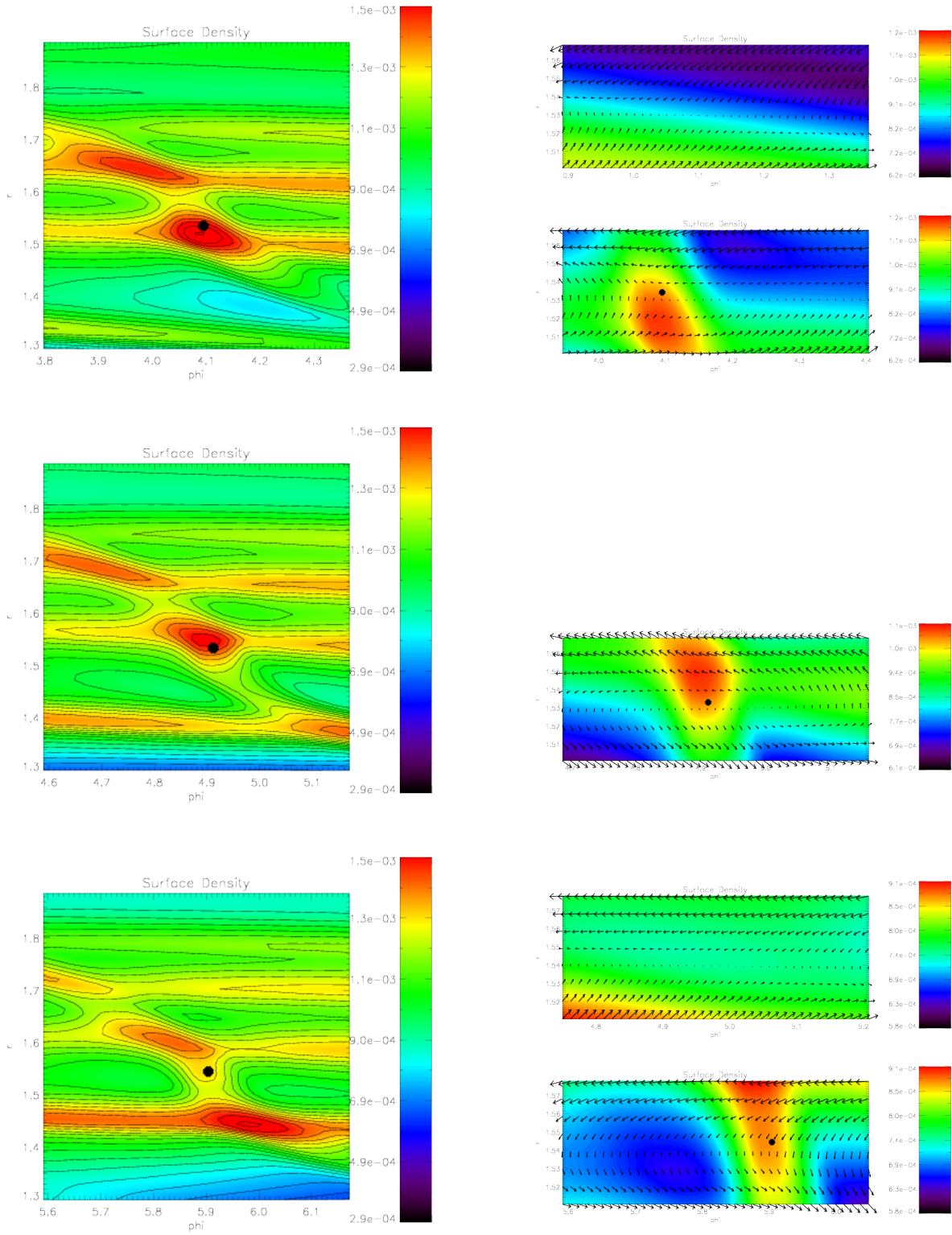


Figure 4. The surface density (left panels) and streamlines in localized disc segments (right panels). The uppermost, middle and lowermost panels correspond to the first, second and third moments of time denoted in the lower right panel of Fig. 2 and Fig. 3.

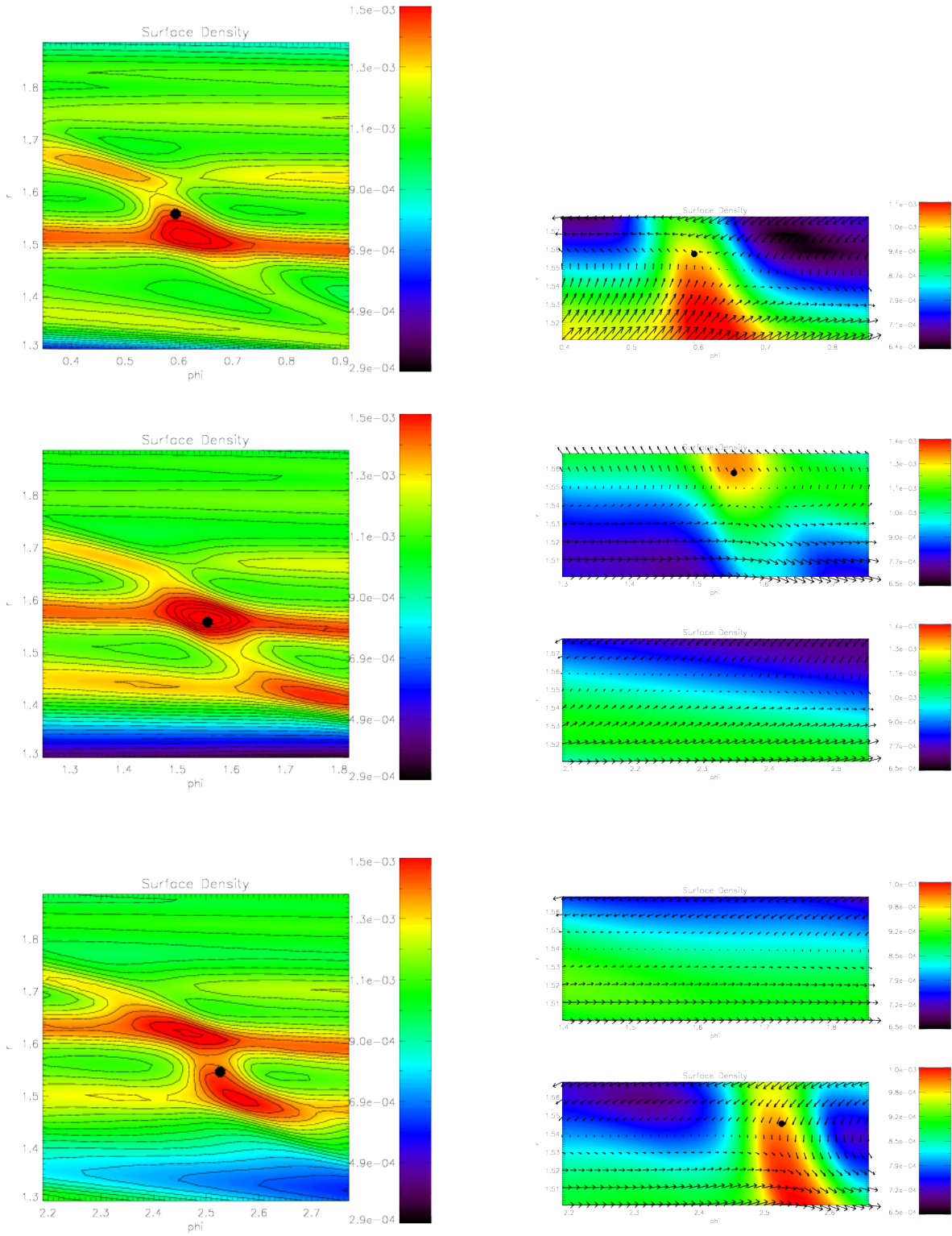


Figure 5. The surface density (left panels) and streamlines in localized disc segments (right panels). The uppermost, middle and lowermost panels correspond to the fourth, fifth and sixth moments of time denoted in the lower right panel of Fig. 2 and Fig. 3.

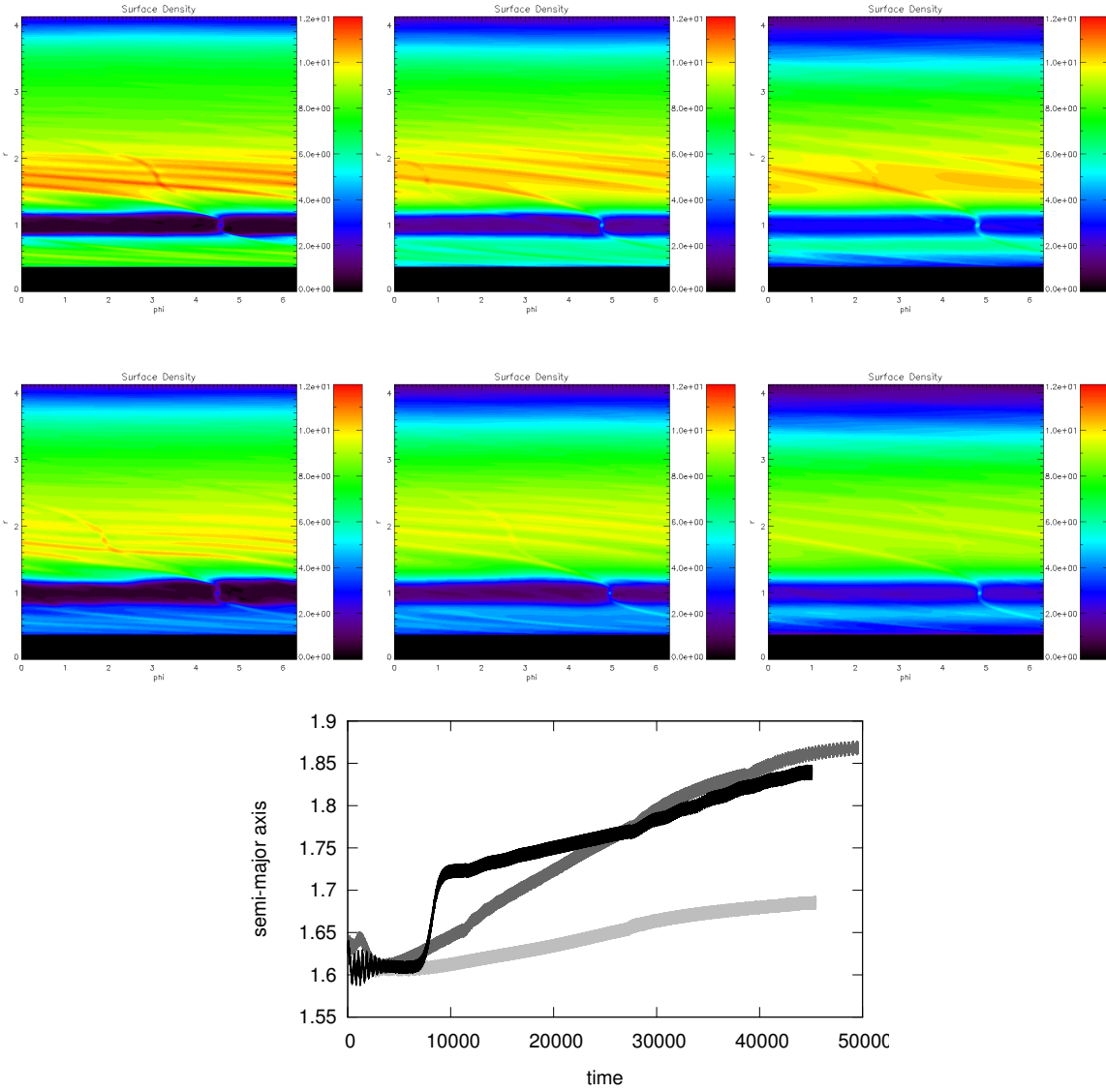


Figure 6. The surface density contours for the disc with aspect ratio $h=0.03$ (left), $h=0.05$ (middle), and $h=0.07$ (right) at two different moments of the evolution, namely at about 10800 time units (three upper panels) and 45000 time units (three middle panels). The density waves weaken at later times because the gap widens and the disk tends to expand outwards along with the super-Earth. The evolution of the semi-major axis of a super-Earth in the disc with aspect ratio $h=0.03$ (black), $h=0.05$ (dark grey), and $h=0.07$ (light grey) (bottom panel).

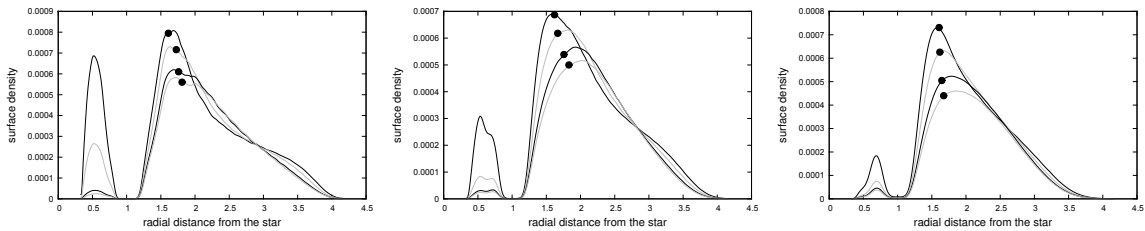


Figure 7. The azimuthally averaged surface density as a function of radius for the disc with aspect ratio $h=0.03$ (left), $h=0.05$ (middle), and $h=0.07$ (right). The position of the super-Earth is indicated by the black dots. The snapshots are taken after 6280, 12556, 25132 and 37600 the time units. The surface density level at the planet location decreases monotonically with time.

that in a balanced state, tidal effects exceed viscous effects with the balance communicated to the super-Earth.

4.2 Interaction of an embedded super-Earth with propagating density waves

It was shown in Podlowska & Szuszkiewicz (2009) that a super-Earth in an orbit exterior to the giant, migrating in the disc towards a Jupiter-mass planet, never got close enough to the giant in order to be caught in a 2:1 commensurability. Before it reached this location, it began to migrate outwards. Let us examine the stage of the evolution when the super-Earth migrates outwards.

We consider a disc with $h = 0.03$, $\nu = 2 \times 10^{-6}$ and $\Sigma_0 = 0.0006$ in dimensionless units. The giant planet was taken to be of one Jupiter mass and the initial orbital radius of the super-Earth was taken to be 1.62. Tests have shown that when the super-Earth is located beyond the 2:1 resonance with the interior giant its migration behaviour is not very much affected by the mutual gravitational interaction of the planets or its initial orbital radius. Accordingly, to clarify that it is the presence of the density waves that induces outward migration, we perform studies in which this interaction is switched off. The interaction of both planets with the central star and the disc remains intact.

The evolution of the semi-major axis of the super-Earth is shown as a function of time in Fig. 1. This shows that after an initial phase in which the semi-major axis decreases on average it eventually increases on average, the transition occurring around $t = 4000$. At this point we emphasize that this ultimate outward migration is not a consequence of the particular disc model or initial conditions adopted (see below).

In order to see how the average torque acting on the super-Earth can then be positive, we consider the behaviour of the semi-major axis of the super-Earth and its distance from the central star. These are plotted for a time span of one typical orbital period of the super-Earth, starting at $t \sim 4906$, where the mean migration rate is outwards, in Fig. 2. In Fig. 2 we also show the torques acting on the super-Earth arising from both the whole disc and only the region located in the domain $1.4 < r < 1.7$ that is close to the planet. The average positive torque exhibited over the one orbital period of the super-Earth occurs for subsequent orbital periods at approximately the same level (see Fig. 1) although the torque itself shows a long period modulation implying some unsteadiness.

We have calculated the values of the torques acting on the planet at seven times which are indicated by the vertical lines in Fig. 2. To illustrate the location of the super-Earth with respect to the density waves excited in the disc by the giant at these times, we indicate the planet positions as seen in a frame that corotates with the giant on the top of the surface density contours at a single moment of time in Fig. 3. Here we remark that the density wave pattern is approximately fixed as seen in a frame that corotates with the giant. Note too that at this time Fig. 3 indicates that the giant planet has migrated inwards to $r \sim 0.9$.

In Figs. 4 - 5 we show the surface density contours in a close vicinity of the planet at the first six times indicated in the lower right panel of Fig. 2. These fall within one orbital period of the super-Earth. We also show the streamlines

both in the vicinity of the planet and for some cases also a coorbital azimuthal domain separated from the planet. This is to confirm that the streamlines do close. For all but the second time, the torque exerted in the vicinity of the super-Earth is positive. Although it is sometimes difficult to discern because of cancellation effects, this is in general seen to be expected from the form of the density contours. For example at the first time there is a surface density excess to the right of the planet that contributes a positive torque, while at the second time there is a surface density excess to the left of the super-Earth that contributes a negative torque.

The coorbital streamlines are closed. At the fourth time they resemble the form associated with steady state horseshoe orbits with an X point near the planet's location. Thus there are oppositely directed turns on either side of the planet. However, because of the presence of density waves the pattern is different in other cases, for example at the first and the sixth times, the planet is inside the circulating region with an X point significantly shifted from the planet at $\phi \sim 1.1$ and 1.5 respectively. Because the situation is a dynamic one, it cannot be said that fluid elements follow these streamlines but they do indicate that they are turned close to the planet at least in some cases. Just as in the standard horseshoe case this is associated with angular momentum exchange with the planet even though the situation is more complex because of the time dependence and the deflection of the streamlines by density waves altering their form.

We have performed a series of simulations in order to investigate the dependence of the outward torque on the physical set up. The evolution of the semi-major axis of a super-Earth for giant planet masses of one Jupiter mass (black curve) and two Jupiter masses (grey curve) is shown in Fig. 1. In these calculations, the gas giant is allowed to migrate and the super-Earth does not interact gravitationally with a gas giant. This ensures that the torque acting on the super-Earth arises entirely from the disc material.

We remark that density wave excitation is expected to be enhanced by placing a more massive giant in the disc. The initial inward migration of the super-Earth is slower in the case with the two Jupiter mass giant. Also in this case, outward migration causes the super-Earth to reach larger radii at equal large times. This is consistent with the idea that the outward torque is produced by some fraction of the outward angular momentum transfer rate associated with density waves excited by the giant. This torque competes with the torques associated with standard type I migration to determine how far the super-Earth can migrate outwards.

We have also performed calculations in which the super-Earth is embedded in discs of different aspect ratio and for which the giant planet was not allowed to migrate.

The pitch of the spiral arms excited by the giant planet depends on the inverse Mach number, or equivalently the aspect ratio $h = H/r$ of the disc. The smaller the aspect ratio the more tightly the spiral arms are wound. In this case the larger Mach number results in the waves more readily becoming nonlinear and forming shocks.

In Fig. 6 we show the disc surface density contours for discs with aspect ratio $h = 0.03$ (left panel), $h = 0.05$ (middle panel), and $h = 0.07$ (right panel) for a one Jupiter mass giant planet. The snapshots are taken after 10800 and 45000 time units. It can be seen that as the aspect ratio

increases, the density waves launched by the giant planet become weaker and less tightly wound.

The migration of the super-Earth in these three different environments is shown in Fig. 6 (bottom panel). The initial orbital radius was 1.64 in each case. The black curve shows the evolution of the semi-major axis of the super-Earth embedded in the disc with aspect ratio 0.03, the dark grey curve in the disc with $h = 0.05$, and the light grey curve in the disc with aspect ratio 0.07.

For the disc with $h = 0.03$ the interaction of the nonlinear density waves with the super-Earth causes it to increase its radius from $r = 1.6$ to $r = 1.72$ in approximately 4000 time units. For the disc with $h = 0.05$ the density waves are weaker and interact with the planet less strongly than in the previous case. Indeed, the outward migration is not so fast and proceeds almost at the same rate during the whole evolution. For the $h = 0.07$ the density waves are even weaker as is their interaction with the planet with the result that it migrates outward very slowly.

To complete our discussion of these simulations we present the azimuthally averaged surface density at different times during the dynamical evolution of the super-Earth for the discs with the different aspect ratios. They are shown in Fig. 7 after 6280, 12556, 25132 and 37600 time units. The azimuthally averaged surface density at the planet location decreases monotonically with time. The planets continue to migrate outwards but they remain in the neighbourhood of the azimuthally averaged surface density maximum in all these runs. This is an indication that the angular momentum transfer due to the density waves continues to widen the gap as well as move the planet outwards. This might be expected if a positive torque acting on the planet requires a non zero outward angular momentum flux carried in density waves. The presence of such a flux might be expected to be associated with gap production interior to the planet.

In Section 5 we study the effect of density waves on planet migration by doing a local calculation of a planet in the presence of forced waves. This approach has the advantage that a very deep gap does not necessarily result. However, the forcing of the planet is similar to what we see in discs where the waves are excited by a giant planet. Thus we gain a strong indication in favour of the hypothesis that the outward migration studied here is a consequence of the direct interaction of a low-mass planet with the spiral waves.

We have also investigated how the evolution of the super-Earth depends on its initial location in the disc. In the left panel of Fig. 8 we show the results of simulations for which the initial orbital radii were 1.64 and 1.9. These show that regardless of the initial orbital radius, the radial position of the planet always approaches the same curve.

Another important issue is the dependence of the migration behaviour of a low-mass planet on its mass. For this purpose we have performed simulations with embedded planet masses of one Earth mass, 5.5 Earth masses, and 10 Earth masses embedded in a disc with aspect ratio $h = 0.03$. Their initial orbital radii were 1.64. The results are also shown in Fig. 8 (right panel). The giant planet, of one Jupiter mass, is not allowed to migrate and, as previously, the planets don't interact with each other gravitationally. The results differ from what would be expected assuming that the outward torque occurs as a direct result of interaction with the spiral wave. In that case it would be proportional to the planet

mass. As the torques arising from disc planet interactions are proportional to the square of the mass in the linear regime, the planet with the lowest mass should be pushed out the most rapidly. This is not the case in our calculations, which indicate the opposite in the early stages.

All the numerical experiments discussed so far indicate that low-mass planets reverse their inward migration at a location, which is very close to a strongly peaked azimuthally averaged surface density maximum. This feature of our calculations appears due to the particular choice of the initial standard surface density profile Eq.(4). To illustrate this, we replace this profile by the more extensive one given by Eq.(5). The outer edge of this disc is now far enough away so that it does not affect the surface density distribution in the vicinity of the planet. The initial profile incorporates a gap so that we eliminate the surface density bumps that appear at gap edges as a result of the gap opening process. In Fig. 9 we show the evolution of the semi-major axis of a planet that starts from the initial value of 1.9, in both the standard disc and the more extensive disc given by Eq.(5). The aspect ratio is taken to be $h = 0.05$ in both cases. The azimuthally averaged surface density profiles for these two cases are shown in Fig. 10. The snapshots are taken after 3100, 6200 and 10000 time units. At the last time there is slow outward migration in both cases. There is a significant difference in the behaviour of the super-Earth migration. The super-Earth initially migrates much more slowly in the case starting with surface density distribution given by Eq. (5), which is in line with the behaviour of standard corotation torques which are expected to be stronger for the case with more rapidly decreasing azimuthally averaged surface density (eg. Masset et al. 2006; Paardekooper & Papaloizou 2009a). However, it could also be a consequence of the tidal effects of the giant being less effective at larger radii in that case.

Let us see how the results of our previous experiments depend on the adopted surface density profile of the disc. In the left panel of Fig. 11 we show the evolution of the semi-major axis of the super-Earth for gas giant masses of one Jupiter mass and two Jupiter masses. As before, other things being equal, the super-Earth outward migration rate is larger if the gas giant has a larger mass.

Now, we come back to the simulations carried out for three different masses of the low-mass planet (Fig. 8) and redo them starting with the more extensive surface density profile Eq.(5). We present a comparison of the evolution of planets with masses 1, 5.5 and 10 Earth masses in a disc with aspect ratio $h = 0.05$. In Fig. 11 (right panel) we show the evolution of their semi-major axes. We see that the larger is the mass of the planet, the greater is the extent of the initial inward migration and the larger the mass of the planet, the faster is the subsequent outward migration. The second of these conclusions could be inferred from the previously discussed low-mass planet evolution in the disc with the standard initial surface density profile (Fig. 8) immediately after the reversal of the direction of the migration.

4.3 The effect of varying viscosity

We have checked that the similar results as found above occur for viscosity ν in the normally considered range $\nu \leq 10^{-5}$. For example Fig. 12 compares the migration be-

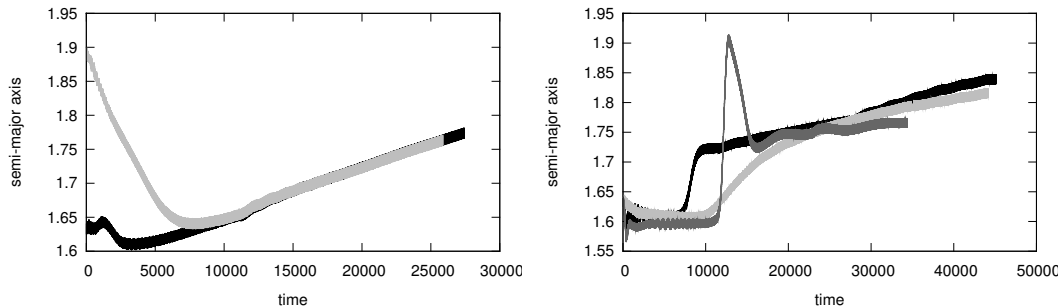


Figure 8. The left panel shows the evolution of the semi-major axis of a 5.5 Earth mass planet for which the initial distance from the central mass was 1.64 (black line) and 1.9 (grey line). The aspect ratio of the disc is $h=0.05$. The right panel shows the evolution of the semi-major axis of a low mass planet with a mass of 1 Earth mass (light grey curve), 5.5 Earth masses (black curve) and 10 Earth masses (dark grey curve). The disc aspect ratio $h = 0.03$.

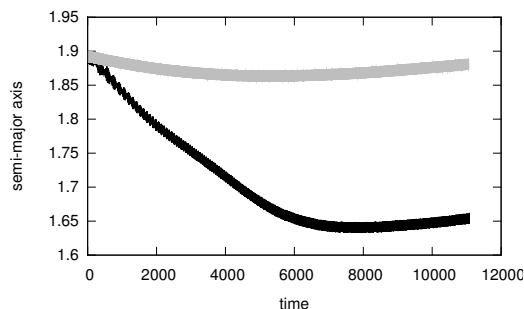


Figure 9. The evolution of the semi-major axis of a super-Earth in a disc with standard initial surface density distribution (black curve) and in a disc with the more extensive initial surface density distribution (grey curve).

haviour and azimuthally averaged surface density profile at $t = 12000$ for $\nu = 2 \times 10^{-6}$ and $\nu = 10^{-5}$. For these simulations the giant planet was one Jupiter mass and they were initiated with the extended surface density profile.

The surface density profile is smoother in the case with larger viscosity and as might be expected, more material leaks interior to the giant planet orbit in this case.

We have also confirmed that similar stalled or outward migration occurs when the applied viscosity is set to zero. We remark that De Val-Borro et al. (2007) find that numerical diffusion in NIRVANA under conditions like those adopted here corresponds to at most $\nu \sim 10^{-7}$ at a particular grid location, while usually amounting to much less. Thus the lack of the smoothing effect provided by even a small applied viscosity results in an initial condition dependent oscillatory form for the azimuthally averaged surface density profile beyond the gap that comes about from the angular momentum transport induced by the tidal effect of the giant planet acting on the initial disc. As there is no long term evolution of the outer disc due to the action of an internal viscosity, these features persist. This in turn leads to some differences in the migrational behaviour of the low mass planet when compared to cases with a non zero ν . In these simulations we adopted an initial disc with the extended surface density profile and aspect ratio $h = 0.05$. The mass of the super-Earth was 5.5 Earth masses.

We have considered the case of a non migrating Jupiter mass giant planet with an initial radius for the super-Earth, $r = 1.65$. The results of this simulation as well as the others undertaken with zero applied viscosity are illustrated in the lower panels of Fig. 12. The low mass planet mi-

grated inwards initially but then subsequently halted with radius slightly exceeding 1.6 dimensionless units. This situation could be followed for about 1500 orbits of this planet. Because the azimuthally averaged surface density in these cases has an oscillatory structure as a function of radius, that may result from the effect of density waves being launched at different Lindblad resonances (see eg. Goldreich & Tremaine 1979), we restarted this run after moving the super-Earth to a new radius $r = 2.5$. It was eventually found to migrate inwards but, when compared to the original rate, at a very small and decreasing rate. This indicates the possibility of either reaching $\sim r = 1.6$ or stalling at some point further out. At $r \sim 2$, where inward migration starts to slow, the surface density profile is affected by tidal effects due to the giant planet and thus the migration of the super-Earth can be affected. Finally we ran the same simulation but with the giant planet mass taken to be two Jupiter masses, starting with the same initial surface density profile but with the initial radius for the super-Earth taken to be $r = 2.5$. In this case the initial inward migration stalls at $r \sim 2$ after which the planet undergoes slow outward migration which could be followed for ~ 1000 planet orbits.

We comment that in all of these cases that have sustained interrupted inward migration over long periods of time, we do not see any removal of the effect on an estimated libration time scale for the horseshoe region, as might be anticipated if corotation torques operated in an otherwise quiescent coorbital region. In this context we remark that parameters are comparable to those adopted in Paardekooper & Papaloizou (2008) (see eg. their Fig. 21) with the libration period being 100–200 planet orbits, which is much less than

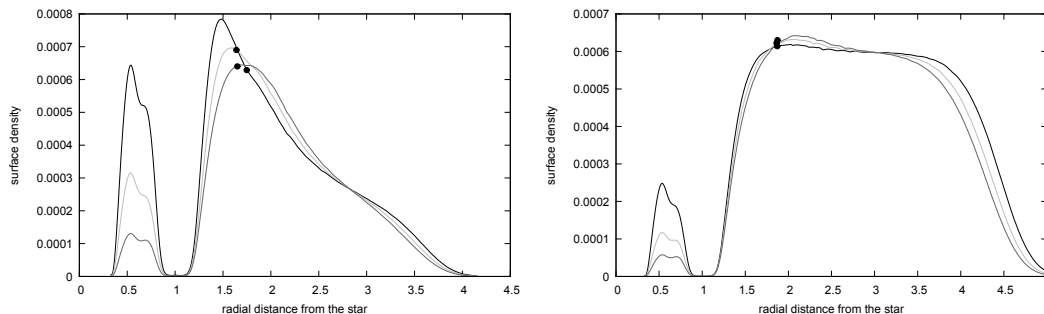


Figure 10. The azimuthally averaged surface density profiles for an initial surface density distribution corresponding to the standard disc (left) and for an initial surface density distribution corresponding to the more extensive disc (right). The snapshots are taken after 3100 (black), 6200 (light grey) and 10000 (dark grey) the time units.

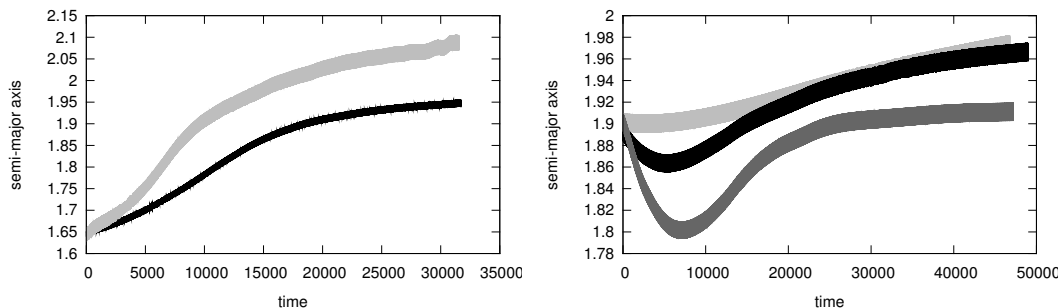


Figure 11. Orbital evolution for simulations starting with the more extensive surface density profile given by equation (5) is illustrated. The left panel shows the evolution of the semi-major axis of a super-Earth in a presence of a gas giant with one Jupiter-mass (black curve) and two Jupiter masses (grey curve). The initial value is 1.65 in each case. The right panel shows the evolution of the semi-major axis of a planet of 1 Earth mass (light grey curve), 5.5 Earth masses (black curve) and 10 Earth masses (dark grey curve) in a disc with aspect ratio $h = 0.05$. The initial value is 1.9 in each case.

the duration of our simulations. A similar situation applies to the inviscid local simulations we have carried out (see the discussion at the end of section 5.2).

4.4 The effect of migration of the giant planet on the migration of the super-Earth

To illustrate the effect on the migration of the super-Earth of allowing the giant planet to migrate, we present the results of a simulation starting with the extended surface density profile, aspect ratio $h=0.05$ and $\nu = 2 \times 10^{-6}$. The mass of the super-Earth was 5.5 Earth masses. Thus this run has the same parameters as for a corresponding one presented in the upper panels of Fig. 12, except that the Jupiter mass planet is allowed to migrate in response to the disc torques acting on it. Results from this simulation are illustrated in Fig. 13.

If effects that interrupt inward migration are associated with the neighbourhood of the giant planet, the super-Earth should naturally tend to move with it. In this case, although the giant moves from $r = 1$ to $r = 0.8$, the super-Earth still moves slowly outwards. However, the ratio of its orbital radius to that of the giant reaches ~ 2 where calculations presented above indicate that tides still operate. Thus the above simulation is approximately consistent with the super-Earth maintaining the same relationship with the giant planet as when it does not migrate.

5 LOCAL SHEARING BOX SIMULATIONS OF A PLANET EMBEDDED IN A DISC WITH INDEPENDENTLY EXCITED DENSITY WAVES

The results obtained in Section 4 for the migration of a super-Earth may be complicated by the presence of a deep gap opened by the gas giant and the particular way that forces density waves in the disc.

To establish the fact that the essential features are a planet embedded in a disc hosting outward propagating density waves, we decided to investigate the phenomenon by performing local simulations with a planet embedded in a disc with density waves independently forced by an independent mechanism that did not involve additional planets producing a very deep gap. These simulations may also be performed at much higher resolution of the coorbital region than the global ones and could be used to show that the qualitative nature of process was robust to changes in parameters such as gravitational softening density wave amplitude and applied viscosity.

5.1 Local Model

We adopt a local Cartesian coordinate system (x, y, z) uniformly rotating with angular velocity $\Omega_p \hat{\mathbf{k}}$ and with origin located at a point where the Keplerian angular velocity is Ω_p as seen in the inertial frame. The local radial coordinate is x and y is the orthogonal coordinate pointing in the di-

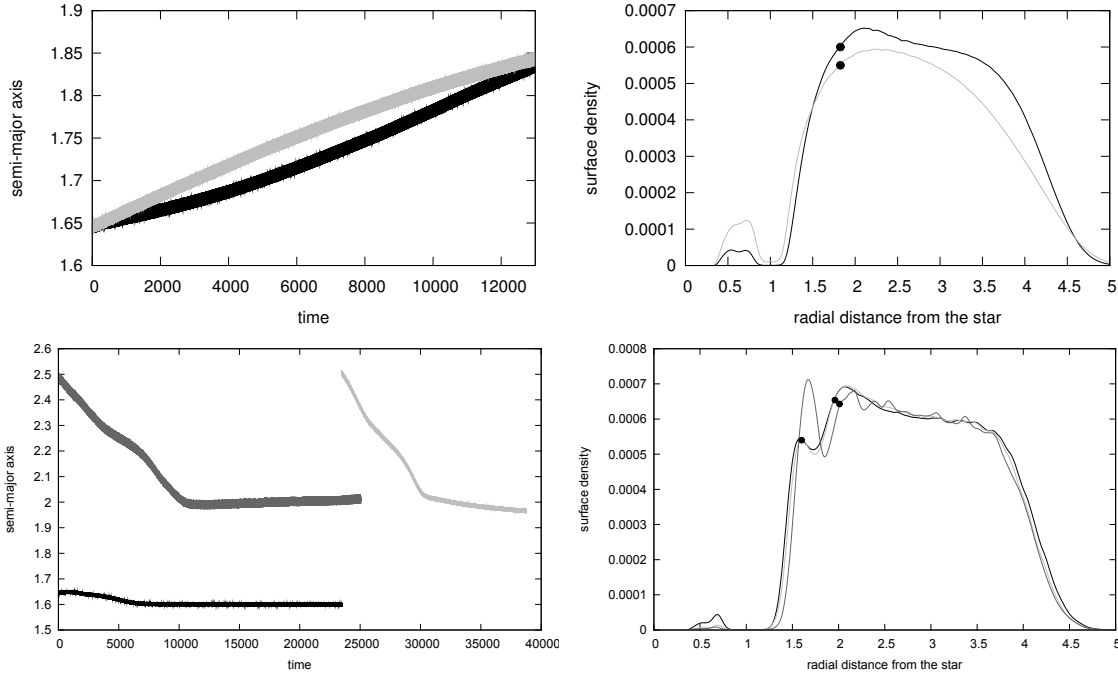


Figure 12. *Upper panels:* The semi-major axis of the super-Earth as a function of time for $\nu = 2 \times 10^{-6}$ (lower black curve) and $\nu = 10^{-5}$ (upper gray curve) is plotted in the left panel. The azimuthally averaged surface density profiles, with the planet position indicated, for $\nu = 2 \times 10^{-6}$ (upper black curve) and $\nu = 10^{-5}$ (lower grey curve) at $t = 12000$ are plotted in the right panel. *Lower panels:* The left panel shows the semi-major axis of the super-Earth as a function of time for the simulations with $\nu = 0$. Results are presented for a one Jupiter mass giant with a super-Earth starting at $r = 1.65$ (black), $r = 2.5$ in a continuation run (light grey) and a two Jupiter mass giant with a super-Earth starting at $r = 2.5$ (dark grey). The right panel shows the azimuthally averaged surface density as a function of radius with the final positions of the planets indicated for the three cases.

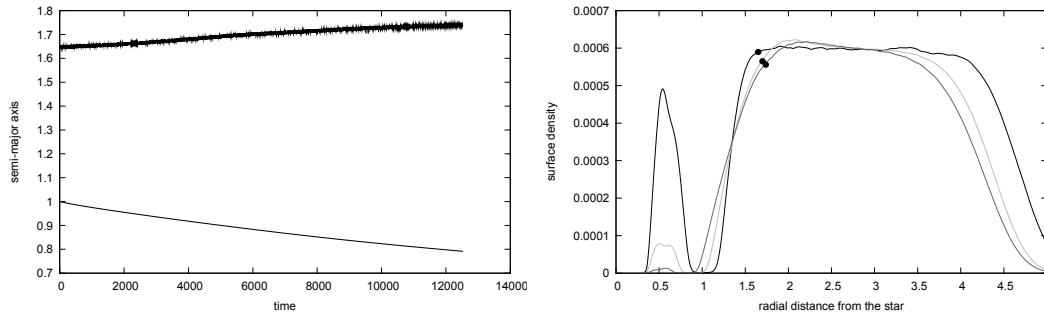


Figure 13. Left: The evolution of the semi-major axes of the super-Earth (upper curve) and the Jupiter mass planet (lower curve) when the latter is allowed to migrate. Right: The azimuthally averaged surface density profiles of the disc after 400 (black), 6000 (light grey) and 12000 (dark grey) time units with the positions of the super-Earth indicated.

rection of the shear. The governing hydrodynamic equations are the continuity equation

$$\frac{\partial \Sigma}{\partial t} = -\nabla \cdot (\Sigma \mathbf{u}), \quad (6)$$

and the equation of motion

$$\frac{\partial \mathbf{u}}{\partial t} + \mathbf{u} \cdot \nabla \mathbf{u} + 2\Omega_p \hat{\mathbf{k}} \wedge \mathbf{u} = 3\Omega_p^2 x \hat{\mathbf{i}} - \frac{1}{\Sigma} \nabla P - \nabla \Phi + \mathbf{f}_\nu, \quad (7)$$

where $\hat{\mathbf{i}}$ is the unit vector in the x direction. The gravitational potential, Φ , for these simulations, is taken to be due to the single planet of mass M_2 , assumed to be fixed at the origin of the rotating coordinate system, and the action of a specified external forcing potential Φ_{ext} . The potential due

to the planet is given by

$$\begin{aligned} \Phi_p &= -\frac{GM_2}{\sqrt{x^2 + y^2 + \epsilon_2^2}} + \Phi_{ext}, \quad x^2 + y^2 < d_{max}^2, \text{ and} \\ \Phi_p &= -\frac{GM_2}{\sqrt{d_{max}^2 + \epsilon_2^2}} + \Phi_{ext}, \quad x^2 + y^2 > d_{max}^2. \end{aligned} \quad (8)$$

The simulations we undertake are two dimensional with no vertical dependence, and the gravitational potential is chosen to be consistent with this. We remark that the indirect term and self-gravity are neglected in this model and as before ϵ_2 is the gravitational softening length for the planet potential. For the simulations reported in detail here we adopted $\epsilon_2 = 0.3H$ and $d_{max} = 3H$. The simulation set up is similar to that described in Papanoizou et al. (2004) with

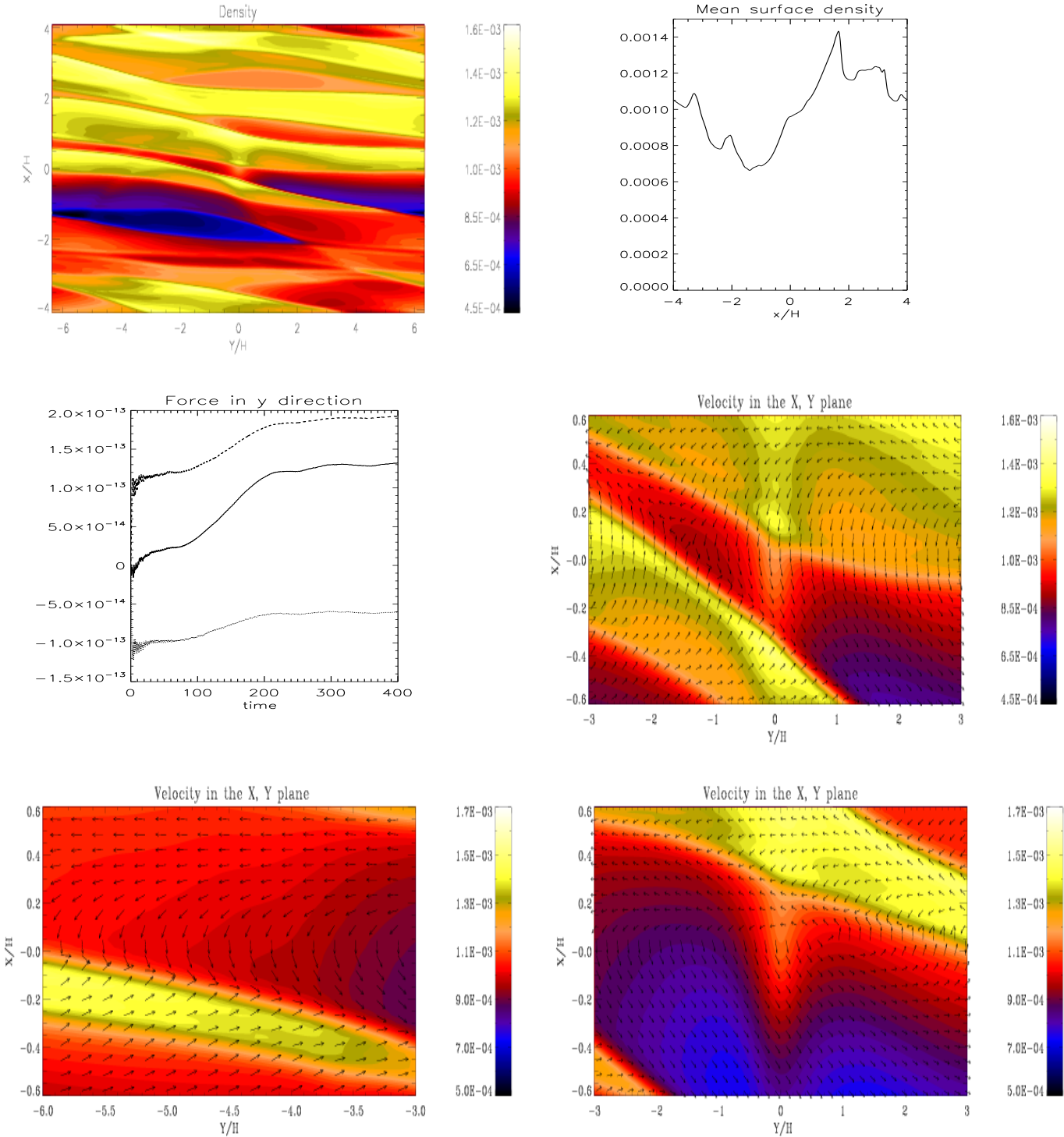


Figure 14. Results are shown for the case with $q = 0.1$, $C_0 = 0.2$, and no applied viscosity, ($\nu = 0$). The upper left panel shows surface density contours 48 orbits after initiation. The upper right panel shows the mean surface density profile averaged over the y direction 56 orbits after initiation. The units are such that the uniform initial value for all local simulations was 0.001. The central left panel shows force components in the y direction acting on the planet evaluated as a running time average. The units are arbitrary but the same for all local simulations illustrated. The uppermost plot gives the contribution from $x < 0$. The lowermost plot gives the contribution from $x > 0$. The central plot shows the total force component in the y direction acting on the planet due to material in the computational domain. The central right hand panel indicates streamlines superposed on surface density contours for the domain $-3 < y/H < 3$ and $-0.6 < x/H < 0.6$ 48 orbits after initiation. The lower left panel indicates streamlines superposed on surface density contours for the domain $-6 < y/H < -3$ and $-0.6 < x/H < 0.6$ 56 orbits after initiation. The right hand panel gives the corresponding plot for $-3 < y/H < 3$ and $-0.6 < x/H < 0.6$.

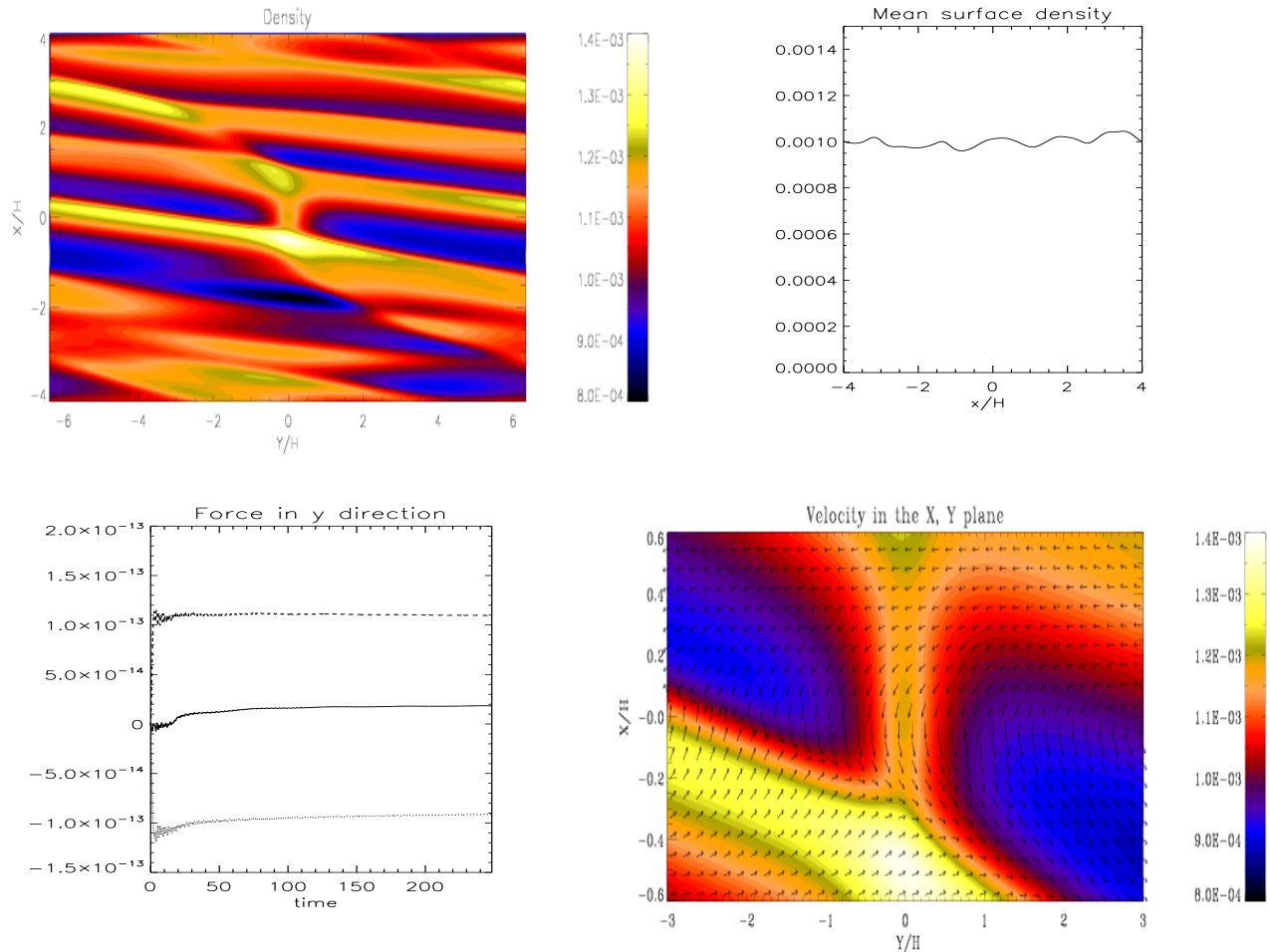


Figure 15. Results are shown for the case with $q = 0.1$, $C_0 = 0.1$, and $\nu/(H^2\Omega_p) = 0.02$. The upper left panel shows surface density contours 48 orbits after initiation. The upper right panel shows the mean surface density profile averaged over the y direction 48 orbits after initiation. The lower left panel shows force components in the y direction acting on the planet evaluated as a running time average. The uppermost plot gives the contribution from $x < 0$. The lowermost plot gives the contribution from $x > 0$. The central plot shows the total force component in the y direction acting on the planet due to material in the computational domain. The lower right hand panel indicates streamlines superposed on surface density contours for the domain $-3 < y/H < 3$ and $-0.6 < x/H < 0.6$ 48 orbits after initiation.

the adoption of the boundary condition that the solution be periodic in shearing coordinates. The distance scale, d_{max} , is used to flatten the planet potential for $x^2 + y^2 > d_{max}^2$ in order to make it effectively periodic in shearing coordinates when applied to the computational domain. The length scale is H , which as for the global models, can be regarded as the putative local disc semi-thickness. The equation of state is thus strictly isothermal with $P = \Sigma H^2 \Omega_p^2$. The viscous force per unit mass, \mathbf{f}_ν , is taken to be the standard Navier Stokes form with kinematic viscosity ν as in the global simulations.

The planet mass appears only through specification of the dimensionless ratio $q \equiv (M_2/M_*)/h^3$ (Papaloizou et al. 2004) which has to be specified for each simulation. Because all lengths are expressed in terms of H and times in units of Ω_p^{-1} , no other parameters need to be specified. However, when M_* is specified, the aspect ratio $h \equiv H/R$ can be found once, R , the orbital radius of the origin of the coordinate system is in turn found from Kepler's law in the form $R^3 = GM_*/\Omega_p^2$.

The computational domain was a rectangle of side $8H$ in the x direction and $4\pi H$ in the y direction. We adopt the convention that the positive x direction corresponds to the outward or outer direction and the opposite direction to the inward or inner direction. We have performed simulations with the equally spaced grid resolutions $(N_x, N_y) = (261, 300)$ which we refer to as the standard resolution and also $(N_x, N_y) = (522, 600)$, which we refer to as higher resolution, in order to confirm convergence of the results. Calculations were initiated with a uniform surface density and velocity $\mathbf{u} = (0, -3\Omega_p x/2, 0)$ corresponding to local Keplerian shear. The external forcing potential was applied in order to excite density waves and so for these simulations plays the role of the giant planet. For $0 < x - x_{min} < 2H$, we adopted the form

$$\Phi_{ext} = C_0 \Omega_p^2 H^2 \sin(\pi(x - x_{min})/(2H)) \times \cos((y - y_{min} - v_{wave}t)/(2H)), \quad (9)$$

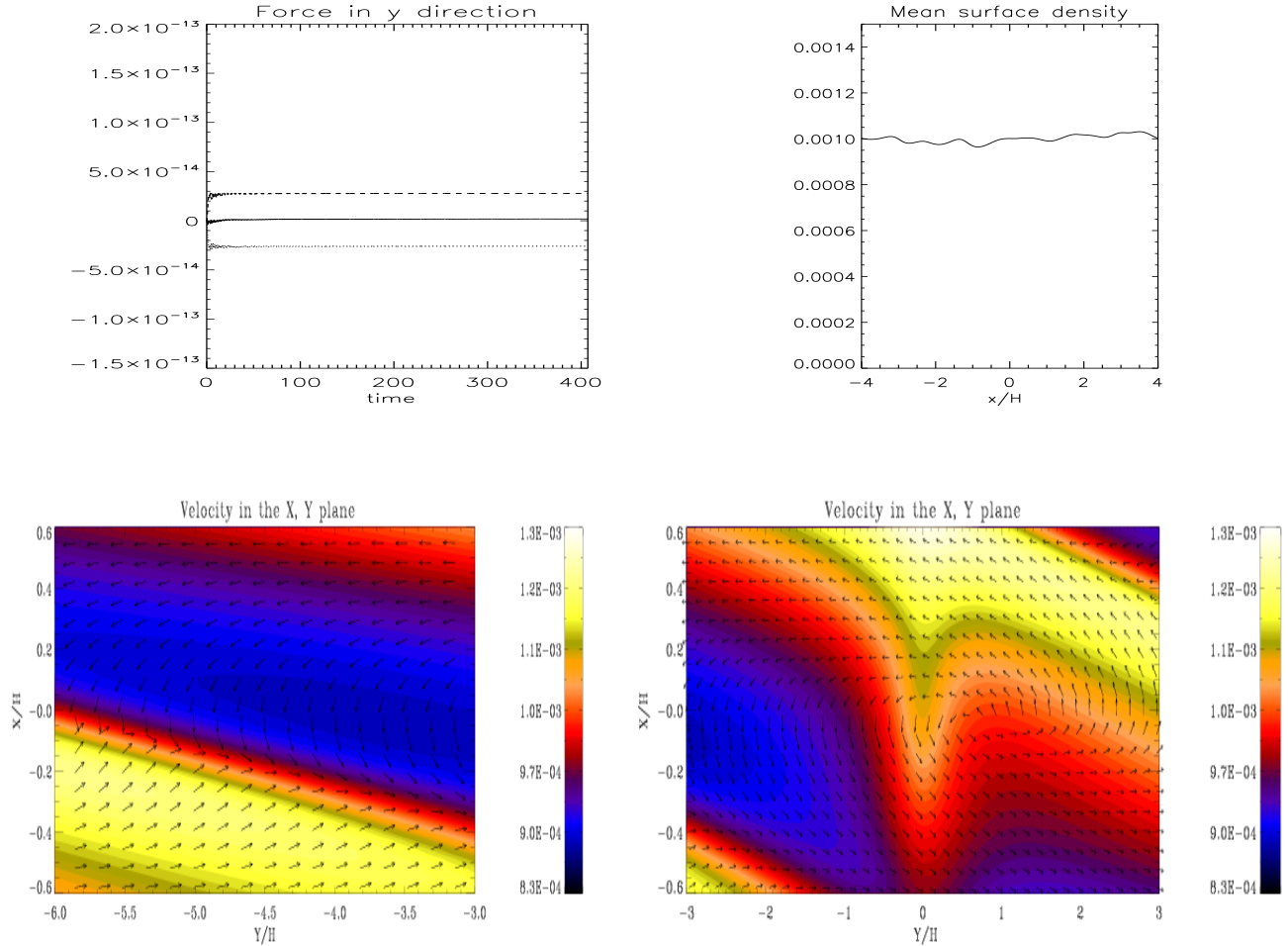


Figure 16. Results are shown for the case with $q = 0.05$, $C_0 = 0.1$, and $\nu/(H^2\Omega_p) = 0.02$. The upper left panel shows force components in the y direction acting on the planet evaluated as a running time average. The uppermost plot gives the contribution from $x < 0$. The lowermost plot gives the contribution from $x > 0$. The central plot shows the total force component in the y direction acting on the planet due to material in the computational domain. The upper right panel shows the mean surface density profile averaged over the y direction 56 orbits after initiation. The lower left panel indicates streamlines superposed on surface density contours for the domain $-6 < y/H < -3$ and $-0.6 < x/H < 0.6$ 56 orbits after initiation. The right hand panel gives the corresponding plot for $-3 < y/H < 3$ and $-0.6 < x/H < 0.6$.

where x_{min} and y_{min} are respectively the minimum values of x and y in the computational domain, the propagation speed $v_{wave} = (3\pi - 3/2)\Omega_p H$ and C_0 is a scaling constant specified for each simulation. For $x - x_{min} > 2H$ no forcing was applied. This is of the form of a harmonic forcing with a single wavelength in the y direction while being localized in the x direction. It is associated with a propagation speed v_{wave} in the y direction so that there is a pattern speed as seen by the super-Earth which is at rest in the centre of the computational domain. This plays the role of the corresponding pattern speed of the giant planet in the global simulations. For the case we have adopted, the putative material that would comove with the potential perturbation is located at $x = -(2\pi - 1)H$, which is a distance $1.28H$ interior to the inner boundary. Accordingly this mimics a perturbation from an orbiting inner planet. The outer Lindblad resonance is located in the computational domain at a distance $0.21H$ from the inner boundary. For the particular choice of parameters we have made, density waves launched

from the outer Lindblad resonance propagate outwards. As the inner Lindblad resonance is not present effects due to inward propagating waves are minimized as, would be expected if the excitation was indeed due to an inner planet. As the waves propagate across the whole domain without further excitation for $x - x_{min} > 2H$, their dissipation is optimized. This feature also limits the influence of disturbances from the periodic system of boxes that arise through application of the shear periodic boundary conditions.

5.2 Local simulation results

We begin by considering a case with $q = 0.1$, $C_0 = 0.2$, and zero applied Navier-Stokes viscosity. The density profile is the most strongly perturbed in this simulation which was run for $400\Omega_p^{-1}$ time units. Some results are shown in Fig. 14. Surface density contours are shown 48 orbits after initiation. These typically dominated by the trailing waves excited by the potential Φ_{ext} . The wake associated with the

embedded planet can scarcely be seen. The surface density profile averaged over the y direction shows that the excited waves causes momentum and mass transport that results in material moving from inside the planet to outside the planet. Tests have shown that this effect weakens if ν is increased and/or the forcing amplitude C_0 is decreased. We also plot the running time averages of the force components acting on the planet in the y direction. As expected, these show that the contribution from exterior/interior to the planet is decrease/increase the y momentum respectively. For these runs the exterior contribution is always smaller resulting in a net outward force on the planet. In the case of the simulation described above, the net force is 60% of the one sided interior force contribution. Note that these forces convert to torques when scaled by the radius of the centre of the box. Tests show the net force, though always outwards, decreases in magnitude with wave forcing amplitude, planet mass and gravitational softening parameter. It is also important to remark that although the density response is dominated by the forced waves the response of the planet is essential in order to produce a net mean force. The specific mean force is found to tend to zero with the planet mass. We also show the streamlines superposed on surface density contours for the domain $-3 < y/H < 3$ and $-0.6 < x/H < 0.6$ 48 orbits after initiation in Fig. 14. In this case they indicate a structure like that associated with normal horseshoes but the planet is not precisely centered on a separatrix as would be the case if pressure effects were negligible. This type of structure was also seen in global simulations e.g. in the uppermost right panel of Fig. 5 We remark that as for the global simulations the streamline configuration varies with time and so streamlines do not precisely indicate particle trajectories. However, by following fluid elements we have found that material initially with $|x| < 0.25H$ remains close to the planet such that $|x| < \sim 0.5H$ in all simulations, which indicates that the fluid particles do indeed turn. Another streamline configuration we find is illustrated in the domain $-6 < y/H < 3$ and $-0.6 < x/H < 0.6$ 56 orbits after initiation in Fig. 14. In this case the flow is strongly affected by the density waves, being deflected to move parallel to shocks (see lower left panel). This has the consequence that the flow through $x = 0$ is in many places reversed compared to that expected for the usual horseshoe configuration, with separatrix located far from the planet. This type of configuration was also seen in the global simulations as in e.g. the middle right panel of Fig. 4

In order to further illustrate the forces on an embedded planet induced by independently excited density waves we show results from two additional simulations. The first was for the same parameters as above but with an applied Navier-Stokes viscosity given by $\nu/(H^2\Omega_p) = 0.02$. Results for the simulation are presented in Fig. 15. In this case the presence of the wakes due to the embedded planet are more apparent in the surface density contours than the previous case. The mean surface density profile averaged over the y direction 48 orbits after initiation, though showing some oscillatory structure, is generally much flatter. The increased value of ν has resulted in lower amplitude waves with less associated angular momentum transport. The total mean force component in the y direction acting on the planet due to material in the computational domain is positive but about seven times smaller than the previous simula-

tion again because of the smoothing action of viscosity. As for the previous simulation, the streamlines in the domain $-3 < y/H < 3$ and $-0.6 < x/H < 0.6$ 48 orbits after initiation show indications of normal horseshoe turns but the streamlines are distorted by the presence of the waves which cause the planet to be no longer centered on a separatrix and the flow to be parallel to shock fronts.

The second case we consider is the previous one but now we reduce the planet mass to $q = 0.05$. The results are shown in Fig. 16. In this case the running time average of the total force component in the y direction acting on the planet is positive but smaller than for the other simulations we have discussed. The mean surface density profile averaged over the y direction 56 orbits after initiation is flatter. Interestingly the streamlines for the domain $-6 < y/H < 3$ and $-0.6 < x/H < 0.6$ 56 at this time are qualitatively similar to those for the case $\nu = 0$ at the same time.

We remark that we have found, by following an appropriate set of fluid elements, that there is no mean mass flow through the coorbital region of the planet. Although the planet is located on a rising surface density profile in the case with $\nu = 0$, the surface density structure is maintained by density waves rather than by either a mass flow, and/or applied viscous stresses, as needed to maintain the surface density structure in the planet trap of Masset et al. (2006). In addition we note that, although coorbital effects are associated with the forces/torques acting on the planet, it seems that the concept of saturation of corotation resonances significantly affecting the positive force in the y direction, plays no role. For the simulations presented here, such effects should be manifest over a libration or return period which corresponds to a time of 64 units for a distance $0.25H$ from the planet. The mean force behaviour is established more quickly that this and remains for much longer periods of time. The increase of the total force magnitude that occurs on a long time scale when $\nu = 0$ is due to the secular effects associated with angular momentum transport due to the waves.

6 THE MECHANISM LEADING TO OUTWARD MIGRATION OF THE SUPER-EARTH

In the previous sections we have described the results of numerical experiments which indicate that outward migration of a low mass planet may occur in a disc in the presence of density waves excited by a forcing potential, which in the global case was that due to a giant planet. We now consider this process further with the aim of investigating its nature.

6.1 Migration of the super-Earth without the source of density waves

The presence of a gas giant in the close internal orbit interior to that of the low mass planet affects the migration of the low-mass planet halting or reversing its migration. This occurs independently of the inclusion of the direct gravitational interaction between the giant and the super-Earth. Accordingly it must occur through modification of the surface density profile through the action of density waves. If the source of density wave excitation is removed, the low

mass planet should undergo type I migration which in our case is directed inwards. In order to demonstrate this, beyond some point of some of our simulations we set the giant planet mass to zero. The above expectations regarding migration are confirmed. We consider a simulation where the non migrating giant planet mass was one Jupiter mass, the disc aspect ratio was $h = 0.05$, the initial orbital radius of the super-Earth was 1.9 and the initial surface density profile was given by Eq.(5). The giant planet was removed at time $t = 750$.

The form of the migration, with and without the removal of the giant planet, is shown in Fig. 17. This clearly indicates that, when the giant planet is removed, the super-Earth starts to undergo inward migration at a rate similar to that it had initially, whereas when it is retained outward migration is ultimately attained. The right panel shows the azimuthally averaged surface density profiles at the end of both simulations.

The disc surface density contours in both these cases are illustrated in Fig. 18 at time $t = 795$. These are very smooth for the case where the giant planet was removed because of the absence of density waves. Note too that in spite of this, the inner cavity with a region of increasing azimuthally averaged surface density, originally produced by the giant remains and the presence this surface density structure does not affect the inward migration of the low mass planet. This is in contrast to the case when the giant is allowed to migrate inwards, described in section 4.4 The edge profile in that case adjusts in a similar way while outward migration is maintained.

6.2 Angular momentum transport and dissipation

To explore the nature of the positive torques acting on the super-Earth, we consider the relationship between angular momentum flux and energy dissipation due to shocks arising from the density waves within a coorbital annulus. The conservation of angular momentum integrated over azimuth may be written in the form

$$\frac{\partial \rho_j}{\partial t} + \frac{\partial F_j}{\partial r} = \int_0^{2\pi} \Sigma r \mathcal{T} d\varphi \quad (10)$$

Here the rate of angular momentum flow through a circle of radius, r , is

$$F_j = \int_0^{2\pi} \Sigma r^2 v_r v_\varphi d\varphi, \quad (11)$$

the angular momentum per unit length is

$$\rho_j = \int_0^{2\pi} \Sigma r^2 v_\varphi d\varphi \quad (12)$$

and $\mathcal{T} = \mathcal{T}_{gi} + \mathcal{T}_{se}$ is the torque per unit mass acting on the disc which has contributions \mathcal{T}_{gi} and \mathcal{T}_{se} due to the giant and super-Earth respectively. In the above, and also below, for simplicity we neglect the viscous contribution to the fluxes although including this would not affect our later discussion.

Assuming that the forcing due to the giant and super-Earth has pattern speeds $\Omega_{i,0}$ and Ω_p respectively, We may also derive a conservation law in the form

$$\frac{\partial \rho_{Jac}}{\partial t} + \frac{\partial F_{Jac}}{\partial r} = -\epsilon_w + (\Omega_p - \Omega_{i,0}) \int_0^{2\pi} \Sigma r \mathcal{T}_{se} d\varphi. \quad (13)$$

Here

$$\rho_{Jac} = \rho_E - \Omega_{i,0} \rho_j, \quad (14)$$

and

$$F_{Jac} = F_E - \Omega_{i,0} F_j, \quad (15)$$

with the energy flux given by

$$F_E = \int_0^{2\pi} \Sigma r v_r (|v|^2/2 + c_s^2 \ln \Sigma + \Phi) d\varphi, \quad (16)$$

and the energy per unit length given by

$$\rho_E = \int_0^{2\pi} \Sigma r (|v|^2/2 + c_s^2 \ln \Sigma + \Phi) d\varphi. \quad (17)$$

Here, for simplicity we have adopted a strictly isothermal equation of state as adopted in the local simulations. As the coorbital region is of small radial extent this should be a reasonable approximation for the global simulations also.

The rate of energy dissipated per unit length in the radial direction by the density waves is ϵ_w . When ϵ_w and \mathcal{T}_{se} are zero, on integration over the radial domain with vanishing boundary fluxes, Eq.(13) yields the Jacobi invariant for the flow. Noting that ρ_{Jac} is negative, we see that the energy dissipation rate can be balanced either against a negative torque produced on the disc by the super-Earth, or by a rate of increase in the magnitude of ρ_{Jac} locally. The latter corresponds to torquing up the disc matter. Thus shock dissipation can in part be associated with balancing of negative torque on the disc produced by the super-Earth which implies a positive torque acting on and outward migration of the super-Earth. Equation (10) also shows that in an approximate steady state a decreasing outward angular momentum flux can be balanced by a negative torque acting on the disc due to the super-Earth.

We investigate the relationship between F_j and the torque acting on the super-Earth during a simulation performed for the disc with initial surface density profile given by Eq.(5) and $h = 0.05$. The giant planet is one Jupiter mass and the super-Earth is $5.5M_\oplus$. The giant planet is not allowed to migrate while the super-Earth is found to migrate slowly outwards. In Fig. 19 we show the comparison of $-F_j$ with the torque acting on the planet over a time span just exceeding one orbital period of the super-Earth after about $t = 11800$. It is seen that these behave similarly.

We have calculated the torque acting on the planet due to the disc matter located in the vicinity of the planet between $r = 1.6$ and $r = 2.3$, the planet being located at around $r = 1.89$, at the moments of the time indicated by the vertical lines in Fig. 19. In Fig. 20 we present the contours of the surface density and in Fig. 21 we show the azimuthally averaged angular momentum flow rate through a circle of radius r as a function of radius calculated according to Eq.(11) at the same times. Note that, although the average value is positive, the torque values are small on account of cancellation effects. The largest magnitude negative value occurs at the first time on account of a large surface density excess to the left of the planet. The largest positive value occurs at the third time on account of a positive surface density excess close to the planet. The azimuthally averaged angular momentum flow rate through a circle of radius r shows a complicated temporal and spatial dependence on account of the dynamic situation and the interaction of waves excited

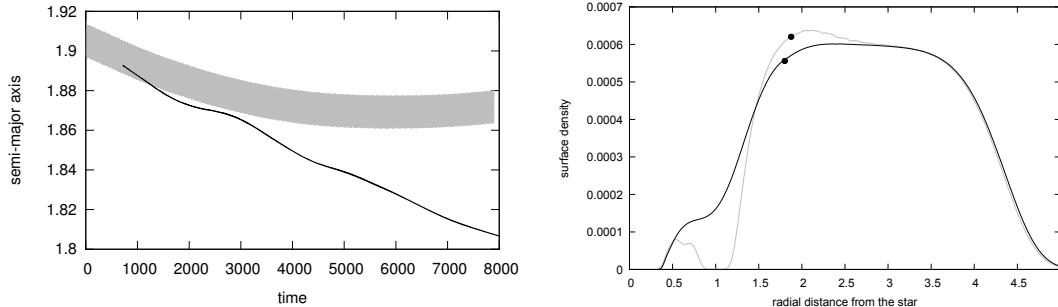


Figure 17. The left panel shows the evolution of the semi-major axis of a low mass planet in the presence of a gas giant (grey curve), and after the gas giant removal from the system (black curve). The right panel shows the azimuthally averaged surface density profiles of the disc for the cases with (grey curve) and without (black curve) a gas giant at the end of simulations (at time $t = 8000$).

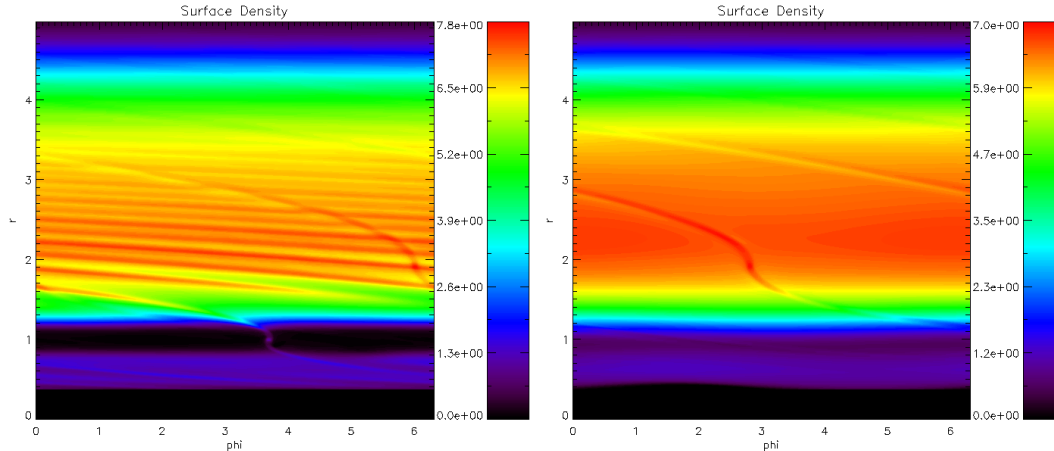


Figure 18. The surface density contours in the disc with waves excited by a gas giant and a super-Earth migrating through them (left) and the surface density distribution in the disc after a gas giant has been removed with a super-Earth migrating in the resulting smooth surface density profile (right).

by the giant and the super-Earth. Nonetheless, we note that Eq.(10) implies that provided F_j vanishes in the gap region, $-F_j(r = 2.3)$ should equal the sum of the torques acting on both planets together with the rate of increase of angular momentum of the disc material (note that this can actually be negative in some places as material does seep across the gap). From Fig. 19 we see that this quantity is of a similar form as the torque on the super-Earth but about three times larger, consistent with the view that some fraction of the angular momentum flow is transmitted to the super-Earth.

7 CONSEQUENCES OF THE WAVE-PLANET INTERACTION FOR THE RESONANCE CAPTURE OF A SUPER-EARTH BY A GAS GIANT

A consequence of the results presented above is that outward migration induced by density waves can prevent an initially inwardly migrating super-Earth from reaching a 2:1 commensurability with the giant. The angular momentum exchange during the super-Earth passage through the density wave field induces its outward migration. It is thus prevented

from approaching close enough to the gas giant's orbit for the commensurability to be reached. From this we expect that in a system with a gas giant we could expect a low mass planet to be in an exterior orbit, possibly close to, but not exactly in 2:1 resonance. There are two observations that relate to our studies. The first is the inference from transit timing variations of a low mass companion of $15M_{\oplus}$ that is close to an exterior 2:1 commensurability with the giant planet ($\approx 2M_J$) in the Wasp-3 system (Maciejewski et al. 2010). However, further observations are needed to confirm this configuration. The other example is found in the GJ876 system where the two outermost planets are close to 2:1 commensurability. The planets have masses $2.27M_J$ and $14.6M_{\oplus}$ so they are within the regime where the mechanism described in this paper can operate. The situation in GJ876 is complex because apart from the configuration of the outer two planets, there is another inner giant in the system with all three planets being in a Laplace resonance. Here we will concentrate on the outer two planets: c and e in the GJ876 system. In order to perform simulations, we scale up the masses of the outer two planets to be 7 Jupiter masses and 43 Earth masses so that with a central star of one solar

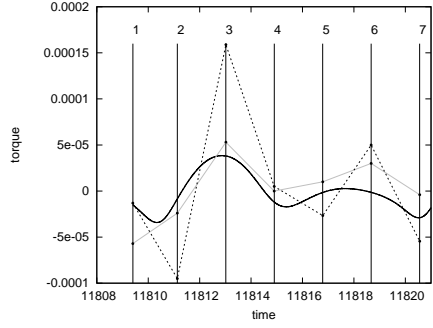


Figure 19. The torque acting on the super-Earth (solid black line), the angular momentum flow rate ($-F_j$) at the position of the super-Earth, across its orbital radius, averaged over azimuth (grey) and $-F_j(r = 2.3)$ averaged over azimuth (dotted). The vertical lines indicate moments of time at which we show the surface density and the azimuthally averaged angular momentum flux as a function of radius below.

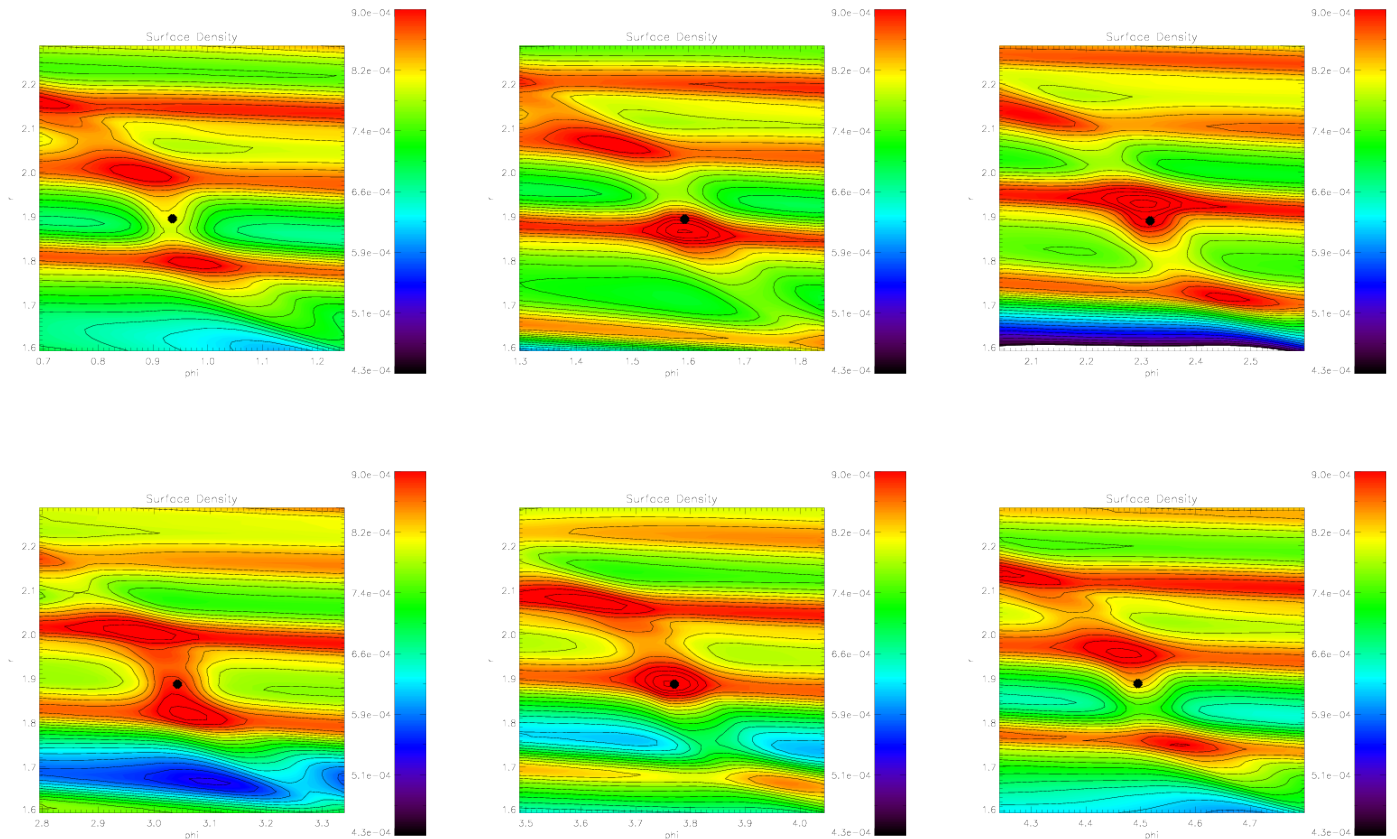


Figure 20. The surface density contours for the first six moments of time progressing from left to right ,upper then lower, marked by vertical lines in Fig. 19.

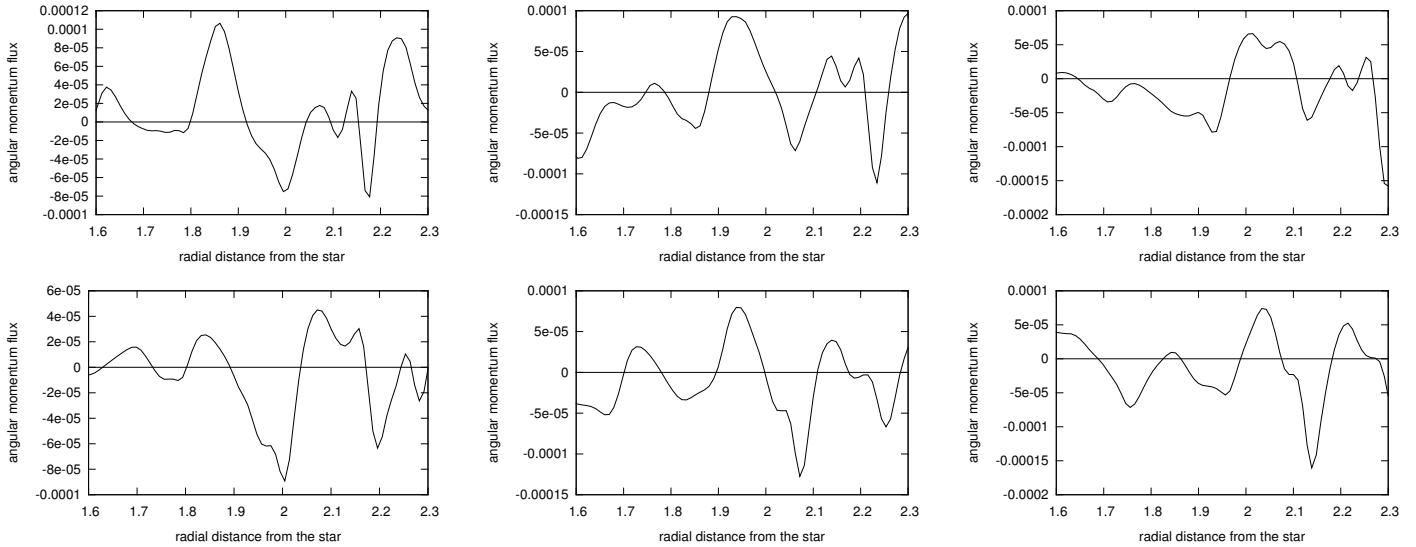


Figure 21. The azimuthally averaged angular momentum flow rate across a circle of radius, r , against radius at the first six moments of time progressing left to right, upper then lower, marked by vertical lines in Fig. 19.

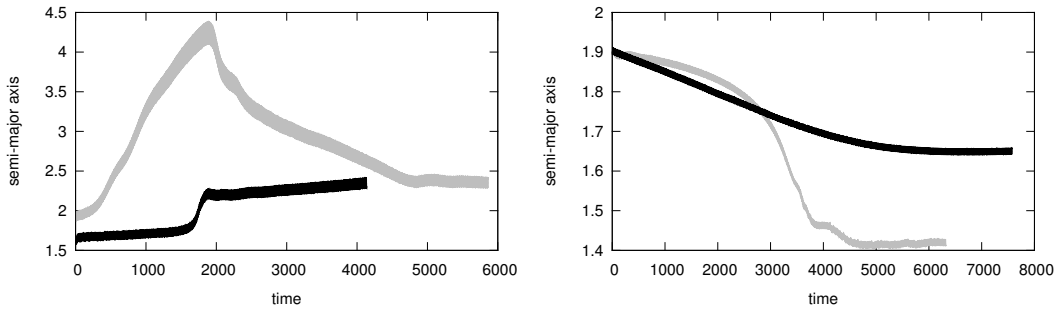


Figure 22. The left panel shows the evolution of the semi-major axis of a $43M_{\oplus}$ planet orbiting exterior to a 7 Jupiter mass gas giant. The initial orbital radius of the super-Earth is $r = 1.9$ (grey curve) and $r = 1.65$ (black curve), respectively. The right panel shows the evolution of the semi-major axis of a $43M_{\oplus}$ (grey curve) and a $20M_{\oplus}$ planet when the giant planet mass was reduced to one Jupiter mass (black curve).

mass, as adopted here, the mass ratios are the same as in the GJ876 system.

In Fig. 22 (left panel) we show the evolution of the semi-major axis of the outermost planet in a disc with aspect ratio $h = 0.05$. In this particular case, the gas giant was not allowed to migrate and the planets do not interact with each other gravitationally. The initial surface density profile was given by Eq.(5). The outermost planet was started in an exterior orbit outside the 2:1 resonance. The evolution proceeds differently for different initial locations in the disc, but the final outcome of the evolution is similar. The smaller planet always ends up at the same radial location, exterior to the 2:1 commensurability with semi-major axis exceeding twice that of the giant. This is illustrated in Fig. 22 for initial locations of the planet of $r = 1.65$ and $r = 1.9$.

In order to explore this issue further, in Fig. 22 (right panel) we compare the behaviour of $43M_{\oplus}$ and $20M_{\oplus}$ planets in the same initial disc but in the presence of a lower mass gas giant with a mass of 1 Jupiter mass. The Jupiter mass planet launches weaker density waves than the 7 Jupiter mass planet. This enabled the $43M_{\oplus}$ planet to pass through the 2:1 resonance. Thus the density waves are too weak to prevent the attainment of the commensurability in this case.

However the $20M_{\oplus}$ planet stopped its migration just exterior to resonance which indicates that smaller mass planets do not reach the commensurability.

Finally, the above simulation for the $43M_{\oplus}$ planet was repeated with the gravitational interaction between the planets included so that capture into the 2:1 resonance takes place. This is illustrated in Fig. 23 where we show the evolution of the semi-major axis of the low mass planet, both resonant angles (see e.g. Papaloizou & Szuszkiewicz 2005, for definitions) and the difference in the mean longitudes.

Thus resonance capture is only possible for sufficiently low mass giants that are not efficient enough as a source of density waves to halt the inward migration. In order to obtain a resonant configuration for a more massive giant, we slowly increased its mass. However, this had to be done after removal of significant amounts of disc material that could act as a carrier of density waves. For example after about 2300 time units we started to increase the mass of the gas giant as a linear function of time until it reached the mass of $7 M_J$ at a time $t = 3341$. At the beginning of this procedure we instantly modified the surface density profile so as to increase the size of the gap around the giant by

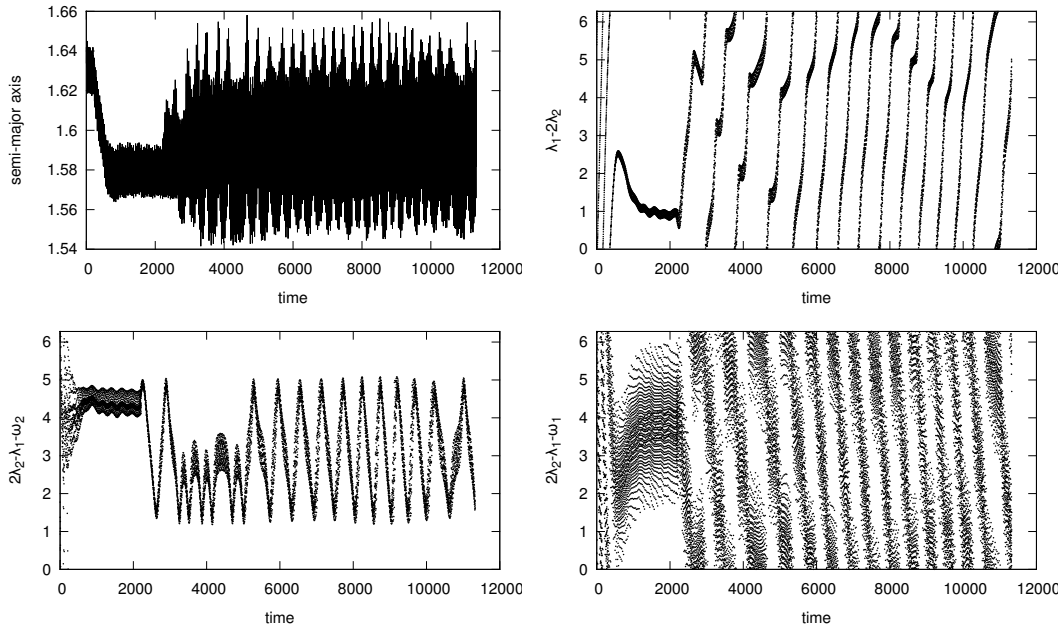


Figure 23. The evolution of the semi-major axis of a $43M_{\oplus}$ planet (upper left panel), both resonant angles (lower panels), and the difference in the mean longitudes (upper right panel) in the presence of the gas giant. After 2300 time units the mass of the giant planet was increased from one to 7 Jupiter masses. The oscillations of the semi-major axis and one of the resonant angles was found to increase in amplitude, and the other angle switches from libration to circulation.

adopting the following modification:

$$\begin{aligned}
 \Sigma &\rightarrow 0.01\Sigma & \text{for } r < 2.4 \\
 \Sigma &\rightarrow \Sigma \times (r/2.5)^{90} & \text{for } 2.4 \leq r < 2.5 \\
 \Sigma &\rightarrow \Sigma & \text{for } r \geq 2.5
 \end{aligned}
 \tag{18}$$

After this has been carried out, the lower mass planet becomes located within an extensive gap, where there is far less material, so that density waves become ineffective at causing it to migrate outwards. Once we started to increase the mass of the gas giant the oscillations of its semi-major axis increased in amplitude and one resonant angle moved from libration to circulation, as can be seen in Fig. 23. However the other resonant continues to librate, but with larger amplitude. These details may depend on the detailed procedure we followed. Nonetheless, the planet remained close to the 2:1 resonance as is observed in the Gliese 876 system (Rivera et al. 2010).

However, the above scenario requires the giant to accrete from a reservoir of material, possibly an interior disc, after having removed most of the nearby outer disc. This would appear unlikely. It may be that the lower mass planet formed after the gas disc had dispersed and/or underwent planetesimal migration (e.g. Raymond et al. 2009) to bring it into a 2:1 commensurability from a larger radius.

8 CONCLUSIONS

In this paper we have studied a new mechanism that can reverse the type I migration of a low mass planet that would occur in an unperturbed locally isothermal gaseous disc. This mechanism operates when there is a source of trailing density waves that propagate through the disc. The most natural example of such source arises from the gravitational perturbation by another planet and for global simulations we have focused on the case when a gas giant is present. We have also carried out local simulations in a shearing box where the forcing was due to an imposed harmonically varying potential with varying amplitude. In all cases the density waves produce shocks which are associated with angular momentum transfer to the disc material. Coorbital disc material then transfers angular momentum to the low mass planet in the same direction, when it is scattered by it. This is analogous to what happens with coorbital material undergoing a slow drag in horseshoe orbits in the case of zero pressure particle dynamics. However, in the cases considered here the dynamics of the coorbital material is not stationary in an appropriately rotating frame and generally more complex. In particular, we stress that although coorbital dynamics plays a role, the situation is unlike that pertaining to standard corotation torques in initially unperturbed discs. For example, because the dissipation and effective drag are produced by shocks, which are viscosity independent and the propagating density waves provide an external source of angular momentum for the coorbital zone, issues of torque saturation become irrelevant. Furthermore although there is an interior gap, the mechanism described here depends on the same source of angular momentum, rather than applied viscous stresses or an accelerating inward accretion flow, to maintain the surface density distribution and in this way it differs from the trap mechanism of Masset et al. (2006).

The effect of the interaction with the density waves is that the migration of a low-mass planet located in an exterior orbit relative to the gas giant can be slowed down and finally reversed. Thus we found that a planet with mass in the super-Earth range cannot approach a Jupiter mass planet close enough in order to form first order mean-motion resonances with it. The migration was found to halt with semi-major axis ranging between 1.6 and 2 times that of the giant. Only when the low mass planet exceeded $\sim 40M_{\oplus}$ was it able to attain a 2:1 commensurability. As the giant planet mass is increased, even larger low mass planets would be required.

Our results indicate that migrating the outermost planet in the GJ876 system to its observed 2:1 commensurability through planet interaction with the gaseous disc alone would be problematic for the reasons outlined above. This may indicate that migration induced by planetesimals after the clearance of the gas disc may have been significant in that case.

ACKNOWLEDGMENTS

This work has been partially supported by NSC Grant No. N N203 583740 (2011-2012) and MNiSW PMN grant - ASTROSIM-PL "Computational Astrophysics. The formation and evolution of structures in the universe: from planets to galaxies" (2008-2011). We acknowledge support from the Isaac Newton Institute programme "Dynamics of Discs and Planets". Part of this research was performed during a stay at the Kavli Institute for Theoretical Physics, and was supported in part by the National Science Foundation under Grant No. PHY05-51164. The simulations reported here were performed using the HAL9000 cluster of the Faculty of Mathematics and Physics of the University of Szczecin. JCBP acknowledges support through STFC grant ST/G002584/1. We wish also to thank Adam Lacy for his helpful comments. Finally, we are indebted to Franco Ferrari for his continuous support in the development of our computational techniques and computer facilities.

REFERENCES

- Adams, F. C., Bloch, A. M., 2009, *ApJ*, 701, 1381
 Artymowicz, P., Clarke, C. J., Lubow, S. H., & Pringle, J. E. 1991, *ApJ*, 370, L35
 Balbus, S. A., Papaloizou, J. C. B., 1999, *ApJ*, 521, 650
 Baruteau, C., Masset, F., 2008, *ApJ*, 672, 1054
 D'Angelo, G., Lubow, S. H., Bate, M. R., 2006, *ApJ*, 652, 1698
 De Val-Borro, M., Artymowicz, P., D'Angelo, G., Peplinski, A., 2007, *A&A*, 471, 1043
 Dermott, S.F., Murray, C.D., Sinclair, A.T., 1980, *Nature*, 284, 309
 Goldreich, P., & Tremaine, S. , 1979, *ApJ*, 233, 857
 Hasegawa, Y., Pudritz, R. E., 2010, *ApJ*, 710, L167
 Johnson, E. T., Goodman, J. & Menou, K. 2006, *ApJ*, 647, 1413
 Kley, W., Bitsch, B., & Klahr, H. 2009, *A&A*, 506, 971
 Kley, W., Crida, A., 2008, *A&A*, 487, L9
 Kley, W., Dirksen, G., 2006, *A&A*, 447, 369
 Laughlin, G., Chambers, J., Fischer, D., 2002, *ApJ*, 579, 455
 Laughlin, G., Steinacker, A., Adams, F.C., 2004, *Astrophys. J.* 608, 489
 Li, H., Lubow, S. H., Li, S., Lin, D. N. C., 2009, *ApJL*, 690, L52
 Lin, D.N.C., Bodenheimer, P., Richardson, D.C., 1996, *Nature*, 380, 606
 Lynden-Bell, D., Kalnajs, A.J., 1972, *MNRAS*, 157, 1
 Maciejewski, G., et al. 2010, *MNRAS*, 407, 2625
 Masset, F. S., 2000, *A&AS*, 141, 165
 Masset, F. S., Morbidelli, A., Crida, A., Ferreira, J., 2006, *ApJ*, 642, 478
 Masset, F. S., Papaloizou, J. C. B., 2003, *ApJ*, 588, 494
 Matsumura, S., Pudritz, R. E., Thommes, E. W., 2005, in *Protostars and Planets V*, Proceedings of the Conference held October 24-28, 2005, in Hilton Waikoloa Village, Hawai'i. LPI Contribution No. 1286., p.8544
 Menou, K., Goodman, J., 2004, *ApJ*, 606, 520
 Nelson R. P., Papaloizou J.C. B., Masset F., Kley W., 2000, *MNRAS*, 318, 18

- Nelson R. P., Papaloizou J.C. B., 2002, MNRAS, 333, L26
 Nelson R. P., Papaloizou J.C. B., 2004, MNRAS, 350, 849
 Ogiwara, M., Duncan, M. J., Ida, S., 2010, ApJ, 721, 1184
 Ogilvie, G. I., & Lubow, S. H. 2003, ApJ, 587, 398
 Paardekooper, S.-J.; Mellema, G., 2006, A& A, 459, L17
 Paardekooper, S.-J.; Papaloizou, J. C. B., 2008, A&A, 485, 877
 Paardekooper, S.-J.; Papaloizou, J. C. B., 2009, MNRAS, 394, 2283
 Paardekooper, S.-J.; Papaloizou, J. C. B., 2009, MNRAS, 394, 2297
 Paardekooper, S.-J., Baruteau, C., Crida, A., Kley, W., MNRAS, 401, 1950
 Paardekooper, S.-J., Baruteau, C., Kley, W., MNRAS, 410, 293
 Papaloizou, J. C. B., 2002, A&A, 388, 615
 Papaloizou, J. C. B., Larwood, J, 2000, MNRAS, 315, 823
 Papaloizou, J. C. B., Nelson, R. P., & Masset, F. 2001, A&A, 366, 263
 Papaloizou, J.C.B., Nelson, R.P. & Snellgrove, M.D., 2004, MNRAS, 350, 829
 Papaloizou, J. C. B., Szuszkiewicz, E., 2005, MNRAS, 363, 153
 Papaloizou, J. C. B., Szuszkiewicz, E., 2010, in *Extrasolar Planets in Multi-Body Systems: Theory and Observations*, K. Goździewski, A. Niedzielski and J. Schneider (eds), EAS Publication Series, 42, 333
 Pierens, A., Nelson, R. P., 2008, A&A, 482, 333
 Podlewska, E., Szuszkiewicz, E., 2008, MNRAS, 386, 1347
 Podlewska, E., Szuszkiewicz, E., 2009, MNRAS, 397, 1995
 Raymond, S.N., Armitage, P. J. & Gorelick, N., 2009, ApJL, L88
 Rivera, E., Laughlin, G., Butler, P., Vogt, S., Haghighipour, N. & Meschiari, S., 2010, ApJ, 719, 890
 Tanaka, H., Takeuchi, T., Ward, W. R., 2002, ApJ, 565, 1257
 Terquem, C., 2003, MNRAS, 341, 1157
 Thommes, E. W., 2005, ApJ, 626, 1033
 Ward, W. R., 1997, Icarus, 126, 261
 Yamada, K., Inaba, S., 2011, MNRAS, 411, 184
 Yu, C., Li, H., Li, S., Lubow, S. H., Lin, D. N. C., 2010, ApJ, 712, 198
 Ziegler U., 1998, Comp. Phys. Commun., 109, 111